Article

Resolving native $GABA_A$ receptor structures from the human brain

https://doi.org/10.1038/s41586-024-08454-1

Received: 30 June 2024

Accepted: 26 November 2024

Published online: 22 January 2025

Check for updates

Jia Zhou[1], Colleen M. Noviello[1], Jinfeng Teng[1], Haley Moore[2], Bradley Lega[3] & Ryan E. Hibbs[1,4]✉

Type A GABA (γ-aminobutyric acid) receptors ($GABA_A$ receptors) mediate most fast inhibitory signalling in the brain and are targets for drugs that treat epilepsy, anxiety, depression and insomnia and for anaesthetics[1,2]. These receptors comprise a complex array of 19 related subunits, which form pentameric ligand-gated ion channels. The composition and structure of native $GABA_A$ receptors in the human brain have been inferred from subunit localization in tissue[1,3], functional measurements and structural analysis from recombinant expression[4–7] and in mice[8]. However, the arrangements of subunits that co-assemble physiologically in native human $GABA_A$ receptors remain unknown. Here we isolated α1 subunit-containing $GABA_A$ receptors from human patients with epilepsy. Using cryo-electron microscopy, we defined a set of 12 native subunit assemblies and their 3D structures. We address inconsistencies between previous native and recombinant approaches, and reveal details of previously undefined subunit interfaces. Drug-like densities in a subset of these interfaces led us to uncover unexpected activity on the $GABA_A$ receptor of antiepileptic drugs and resulted in localization of one of these drugs to the benzodiazepine-binding site. Proteomics and further structural analysis suggest interactions with the auxiliary subunits neuroligin 2 and GARLH4, which localize and modulate $GABA_A$ receptors at inhibitory synapses. This work provides a structural foundation for understanding $GABA_A$ receptor signalling and targeted pharmacology in the human brain.

$GABA_A$ receptors assemble in homo- and hetero-pentameric combinations of subunits. This combinatorial puzzle generates a broad spectrum of sensitivities to the neurotransmitter GABA, channel biophysical properties and drug-binding interfaces[9,10]. The 19 human receptor subunits are α1–6, β1–3, γ1–3, ρ1–3, δ, θ, π and ε[11]. These subunits form a ring surrounding a central ion-conducting channel through the membrane. Binding of GABA to β–α interfaces favours channel opening, which increases chloride conductance and generally acts to inhibit neuronal activity[12]. The α1 subunit exhibits the overall highest expression, and receptors containing α1, β2 and γ2 subunits are thought to be the most abundant[1,13].

Although a large number of subunit combinations is theoretically possible, only a small subset of these is understood to form physiologically relevant $GABA_A$ receptors[1]. In situ hybridization and immunohistochemical approaches have determined the amounts of individual $GABA_A$ subunits in human, non-human primate, and rodent brains[10,13–16]. Several distinct assemblies have been structurally determined using recombinant systems[4–7]. A recent study determined native mouse $GABA_A$ receptor structures[8]. Together, these approaches inform on differences among species and on the likelihood of receptors to contain certain combinations of subunits. However, the absolute arrangements of subunits in human brains remain ambiguous. Notably, the diversity of $GABA_A$ receptor subunit compositions is greater in primates compared with rodents[15], and is even more heterogeneous in humans than in non-human primates[16]. Another important element of native receptor complexity is regulation by auxiliary subunits. The localization, clustering and anchoring of $GABA_A$ receptors are modulated by synaptic proteins, including GARLH proteins, neuroligin 2 (NL2), gephyrin and neurexins[17–20]. Despite their importance, we have almost no structural understanding of how these proteins interact with the intact receptor.

Here we explore the compositions and arrangements of native $GABA_A$ receptors in the human brain using a high-affinity antibody fragment (Fab 1F4, hereafter referred to as 1F4) that targets the α1 subunit, mass spectrometry and cryo-electron microscopy (cryo-EM). We collected tissue samples from 81 patients with temporal or frontal lobe epilepsy, which were pooled into two groups for receptor analysis. Our study revealed a minimum of 12 distinct α1-containing $GABA_A$ receptor assemblies, comprising α1, α2, α3, β1, β2, β3 and γ2 subunits, defining an extensive repertoire of native structures. Several of the structures exhibited drug-like densities at subunit interfaces that led us to uncover modulator activity for two epilepsy drugs that were not previously known to act on the $GABA_A$ receptor. Cryo-EM mapped binding of one of these drugs, lamotrigine, to the α1–γ2 benzodiazepine-binding site. Additionally, we observed non-receptor densities adjacent to an α1–γ2 subunit interface in the transmembrane domain (TMD), suggesting interactions with GARLH4 and NL2, which were supported by mass spectrometry data.

[1]Department of Neurobiology, University of California San Diego, La Jolla, CA, USA. [2]Department of Neuroscience, UT Southwestern Medical Center, Dallas, TX, USA. [3]Departments of Neurological Surgery, Neurology, Psychiatry and the Peter O'Donnell Jr. Brain Institute, UT Southwestern Medical Center, Dallas, TX, USA. [4]Department of Pharmacology, University of California San Diego, La Jolla, CA, USA. ✉e-mail: rehibbs@ucsd.edu

Receptor purification from resected brain tissue

Drug-resistant epilepsy can be treated with surgical resection[21]. This procedure commonly results in the removal of otherwise healthy tissue outside of the epileptic focus that has been verified by histopathology to lack structural abnormalities. To investigate the composition of native $GABA_A$ receptors in the human brain, we used affinity purification with an anti-α1 Fab[22] (1F4) in conjunction with cryo-EM, leveraging nominally healthy neurosurgical specimens obtained from patients with epilepsy. The surgical resections primarily targeted the temporal lobe, with a smaller portion from the frontal lobe; tissues were collected between 2016 and 2023 (Fig. 1a) as detailed in Methods. Tissue samples (0.5–6 g each) were pooled into two groups. The first group contained tissue from 45 individuals, and the second group included tissue from 36 individuals. The pooled samples were from patients ranging from 19 to 77 years of age, of whom 39.5% were women and 60.5% were men. Further details regarding patient demographics can be found in Extended Data Tables 1 and 2.

The resected tissues were homogenized to isolate cell membranes (Fig. 1b). Receptors were then extracted using lauryl maltose neopentyl glycol to preserve interactions with synaptic binding partners[23]. We isolated native $GABA_A$ receptors using 1F4, which targets the α1 subunit, known for its high expression and ability to assemble with other subunits including α2–6, β1–3, γ1–3 and δ[8,24–27]. The purified receptors were then reconstituted into spMSP1D1–lipid nanodiscs[28]. This nanodisc scaffold was selected for its ability to produce larger, circularized nanodiscs, which may minimize artefacts in ion channel conformation[29]. We confirmed the presence of isolated α1-containing $GABA_A$ receptors using mass spectrometry followed by preparation of cryo-EM grids. Thirteen $GABA_A$ receptor subunits were identified by mass spectrometry: α1–6, β1–3, γ1–3 and δ (Fig. 1b and Extended Data Fig. 1a,b). Among them, α1, β2 and γ2 were the most abundant, consistent with reports that these three subunits co-assemble into the most abundant $GABA_A$ receptor pentamer population[1,3]. The highly sensitive mass spectrometry analysis suggests many potential compositions of α1-containing $GABA_A$ receptors in the human brain. However, it does not provide insights into stoichiometries and assemblies.

Heterogeneity in subunit assemblies

To determine the subunit compositions of major α1-containing $GABA_A$ receptor subtypes, we analysed two large single-particle cryo-EM datasets derived from tissue samples from 45 and 36 patients with epilepsy, referred to as datasets 1 and 2, respectively (Extended Data Table 3). The protein samples for both datasets were prepared following the procedures outlined in Fig. 1b, with the dataset 2 sample also undergoing chemical crosslinking to stabilize interactions with synaptic binding partners or auxiliary subunits; this modification resulted in a very minor improvement in map quality but no noticeable differences in receptor conformations. Two-dimensional (2D) classification revealed two major subsets of $GABA_A$ receptor particles: one with receptors bound by two Fab molecules and another with particles bound by a single Fab (Extended Data Figs. 2–4), suggesting the presence of receptors with different numbers of α1 subunits.

We used several rounds of focused three-dimensional (3D) classification, followed by non-uniform refinement to resolve distinct cryo-EM density maps that correspond to unique subunit arrangements of pentameric receptors. The classification was focused on the extracellular domain (ECD), which includes strong asymmetric features such as bound Fabs and subunit-specific N-glycosylation patterns. Ultimately, we obtained a total of 7 distinct cryo-EM density maps from dataset 1 with overall resolutions ranging from 2.5 to 3.3 Å (Fig. 2 and Extended Data Fig. 2), and 7 maps from dataset 2 with overall resolutions of 2.7 to 3.3 Å (Fig. 2 and Extended Data Fig. 3). Three compositions overlapped between the datasets; particles from these subunit assemblies were combined to generate the final maps (Extended Data Fig. 5).

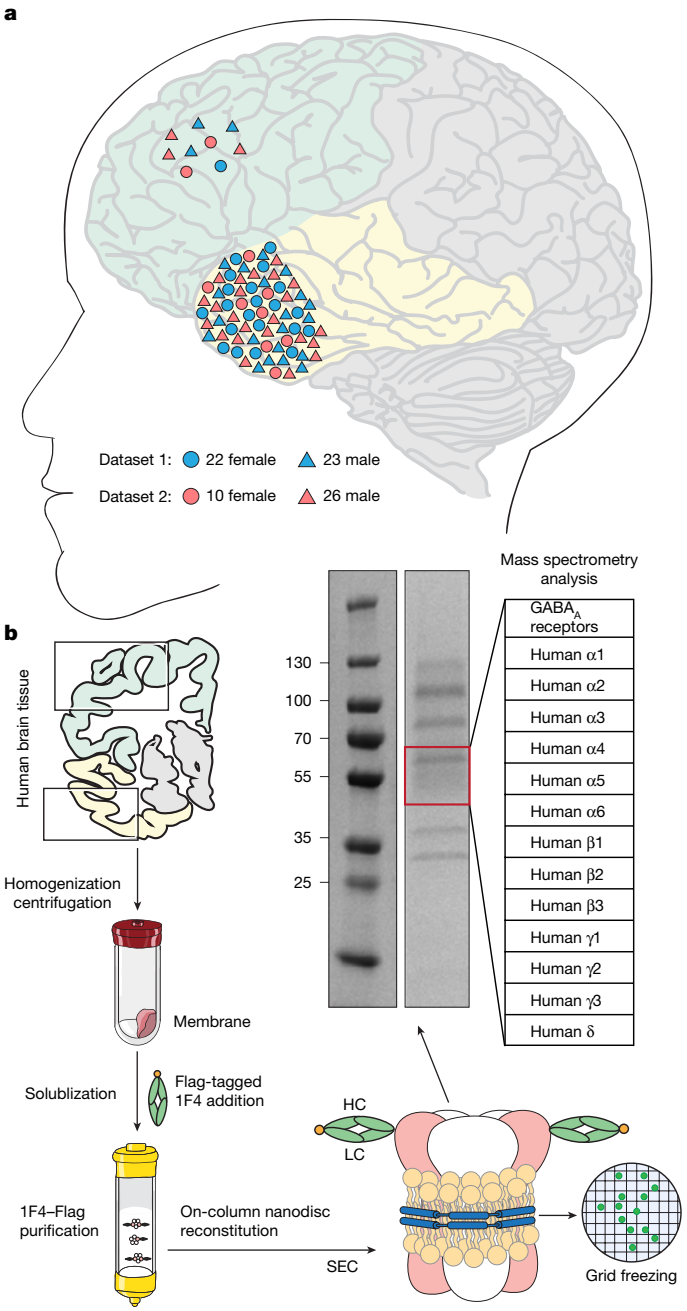

Fig. 1 | Tissue samples and purification of α1-containing $GABA_A$ receptors. **a**, Sample locations and demographics of patients with epilepsy. Green indicates frontal lobe and yellow indicates temporal lobe. Dataset 1 includes 45 patients: 22 women and 23 men. Dataset 2 includes 36 patients: 10 women and 26 men. **b**, Left and bottom, overview of tissue processing and purification of α1-containing $GABA_A$ receptors using Fab 1F4. The brain cross-section is shown with the same colour scheme as in **a**. Middle, the purified $GABA_A$ receptors were separated by SDS–PAGE. Right, subunits identified by mass spectrometry of the region of the gel outlined in red. Gel source data are provided in Supplementary Fig. 1. HC, heavy chain; LC, light chain; SEC, size-exclusion chromatography.

The 11 high-resolution maps enabled distinction of subunits through progressively finer levels of analysis. Subunit identities were first assigned on the basis of selective binding of 1F4 to α1, followed by identification of the distinct N-glycosylation patterns among α, β, γ and δ subunits. The relatively weak density of the γ-subunit TMD[4,8] was further used for coarse identification of subunits. Next, finer

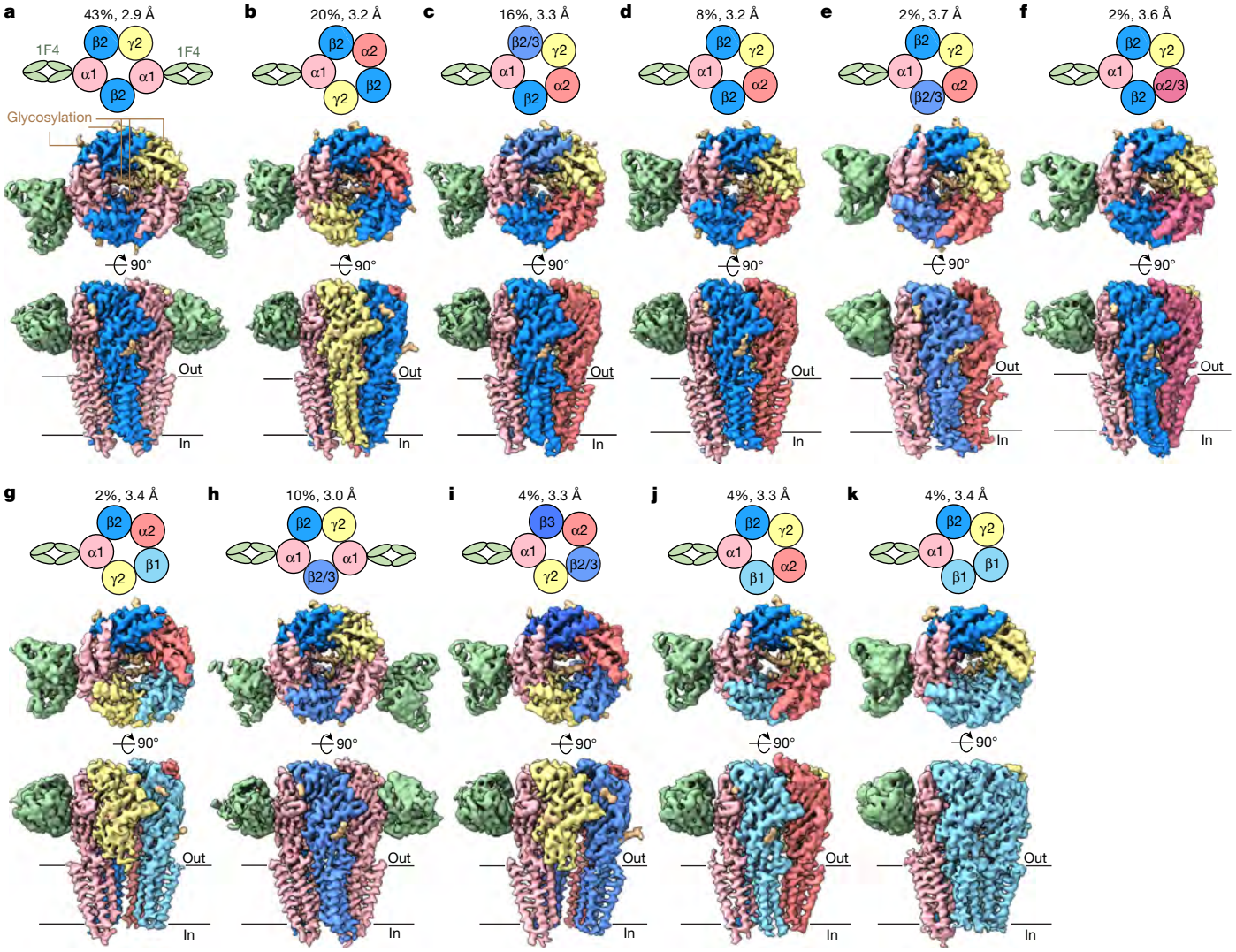

Fig. 2 | Architecture of native human α1-containing $GABA_A$ receptors. **a**–**c**, Cryo-EM maps of the three $GABA_A$ receptor assemblies that are present in both datasets: β2–α1–β2–α1–γ2 (**a**), β2–α1–γ2–β2–α2 (**b**) and β2/3–α1–β2–α2–γ2 (**c**). **d**–**g**, Cryo-EM maps obtained from dataset 1: β2–α1–β2–α2–γ2 (**d**), β2–α1–β2/3–α2–γ2 (**e**), β2–α1–β2–α2/3–γ2 (**f**) and β2–α1–γ2–β1–α2 (**g**). **h**–**k**, Cryo-EM maps obtained from dataset 2: β2–α1–β2/3–α1–γ2 (**h**), β3–α1–γ2–β2/β3–α2 (**i**), β2–α1–β1–α2–γ2 (**j**) and β2–α1–β1–β1–γ2 (**k**). Each panel includes a schematic cartoon illustrating the composition, subunit arrangement and 1F4 binding. It also includes the overall cryo-EM map top and side views, resolution, and percentage. The percentage is derived from the fraction of particles that gave rise to the map of that assembly (Extended Data Figs. 2 and 3).

features were examined: the presence of GABA at β–α interfaces, and the density of residues with side chains that could be unambiguously assigned to receptor subunits (Supplementary Figs. 1–11). In all cases, subunit assignment and 3D classification were performed iteratively, with ambiguity at a subunit position leading to further classification. Five maps indicated the presence of a mixture of two subunits at one position that could not be separated (Fig. 2c,e,f,h,i). In these cases, models corresponding to unique subunit assemblies were built and analysed. In total, these 11 distinct cryo-EM maps enabled building of 12 models of unique subunit assemblies (Extended Data Tables 4 and 5).

The predominant subunit composition in both datasets was β2–α1–β2–α1–γ2 (Fig. 2a, Extended Data Figs. 5a and 6a and Supplementary Fig. 2), aligning with previous functional investigations[1,3] and a recent structural study of the receptor from mouse brain[8]. The receptor conformations among the closely related native and recombinant protein structures showed good agreement (Extended Data Fig. 7). The second most abundant population was β2–α1–γ2–β2–α2, resulting in a previously undefined α2–β2 interface (Fig. 2b, Extended Data Figs. 5b and 6b and Supplementary Fig. 3). Despite being expressed at lower levels than α1 in the brain, α2 holds promise as a drug target for neuropsychiatric illnesses, substance abuse and pain[30]. A similar composition included a mixture of β2 and β3 (β2/3) at one position, resulting in β2/3–α1–β2–α2–γ2 (Fig. 2c, Extended Data Figs. 5c and 6c and Supplementary Fig. 4). To our knowledge, the β3-containing model is the first to report β3 assembling into native α1-containing $GABA_A$ receptors. Despite the close similarity to β2 (80% amino acid identity), β3 has unique functional properties that distinguish it in $GABA_A$ receptor-mediated inhibition[31,32].

Beyond the three major assemblies identified in both datasets (Fig. 2a–c), eight maps were reconstructed uniquely from separate analysis of datasets 1 and 2. Dataset 1 contained an easily distinguishable β2–α1–β2–α2–γ2 assembly that overlapped with one of the mixed compositions common to both datasets (Fig. 2d, Extended Data Fig. 6d and Supplementary Fig. 5). This finding underscores the abundance of receptors comprising both α1 and α2 subunits, and reveals details of receptors with an α2–γ2 benzodiazepine site. Dataset 1 also contained a minor population of β2–α1–β2/3–α2–γ2, indicating rare α1–β3 and β3–α2 subunit interfaces (Fig. 2e, Extended Data Fig. 6e and Supplementary Fig. 6). The compositions containing α3 subunits are also heterogeneous with a clear mixture at one position, β2–α1–β2–α2/3–γ2.

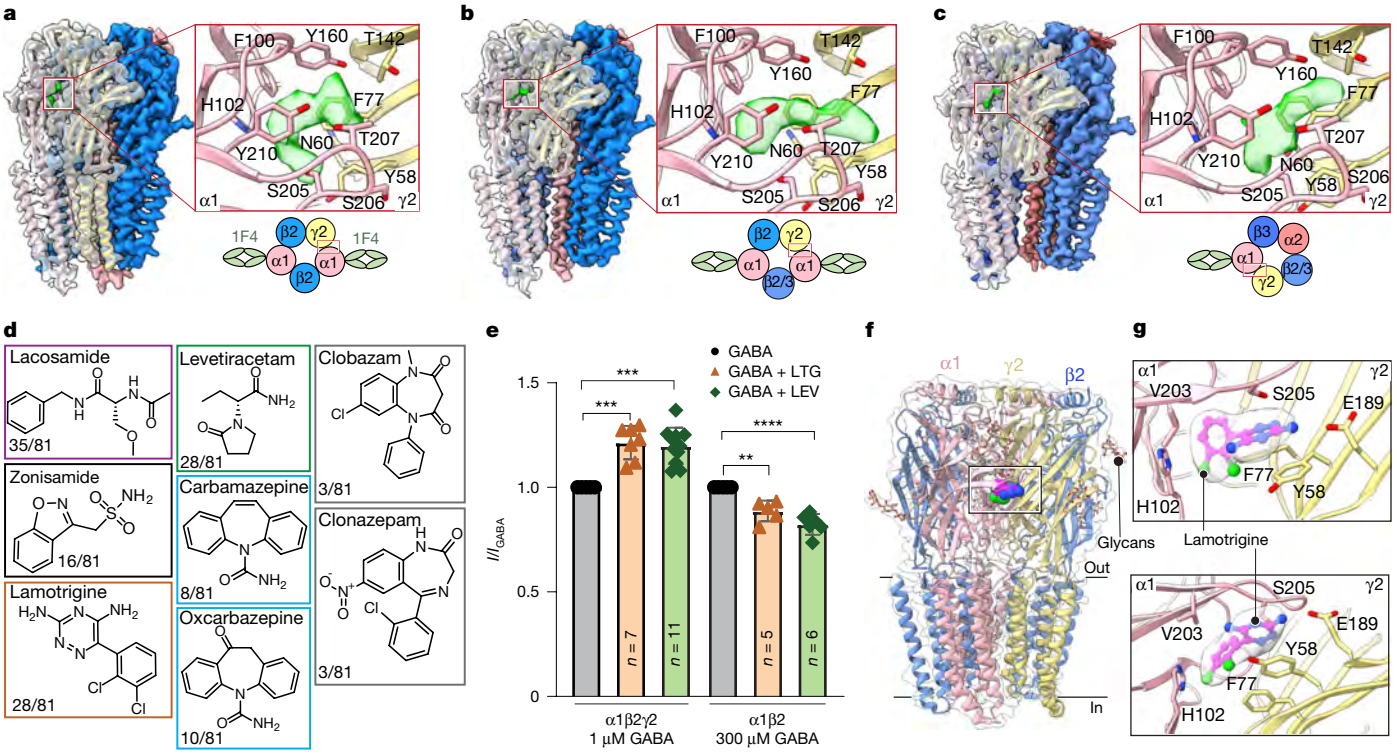

Fig. 3 | Densities in native α1-containing $GABA_A$ receptors and related pharmacology. a–**c**, Cryo-EM densities were observed at the interfaces formed by the ECDs of the α1 and γ2 subunits in β2–α1–β2–α1–γ2 (**a**), β2–α1–β2/3–α1–γ2 (**b**) and β3–α1–γ2–β2/3–α2 (**c**) $GABA_A$ receptors. Thresholds for maps are provided in the Methods. Residues surrounding the density and known determinants of benzodiazepine and DMCM binding are labelled. Experimental density located at the interface is shown as a semi-transparent surface. Each panel includes a schematic illustrating the composition of the receptor. **d**, Chemical structures of six drugs taken by the tissue donors and the fraction of donors who were taking them. **e**, Potentiation of currents produced by GABA plus 50 μM lamotrigine (LTG) and GABA plus 250 μM levetiracetam (LEV) on α1β2γ2 and α1β2 receptors. $n = 7$ (lamotrigine, α1β2γ2), 11 (levetiracetam, α1β2γ2), 5 (lamotrigine, α1β2) and 6 (levetiracetam, α1β2) recordings from independent cells. Data are mean ± s.e.m.; Welch's *t*-test; $^{**}P < 0.01$, $^{***}P < 0.001$, $^{****}P < 0.0001$. **f**, Cryo-EM density map and structural model of the recombinant human $GABA_A$ receptor (β2–α1–β2–α1–γ2) in complex with lamotrigine. Glycans are labelled for clarity. **g**, Close-up views of the lamotrigine-binding pocket, with nearby residues displayed in stick representation.

(Fig. 2f, Extended Data Fig. 6f and Supplementary Fig. 7). The α3 subunit is implicated not only in regulating sleep[33] but also specifically in anxiety, with distinct roles compared with α2[34]. Finally, dataset 1 contains a small fraction of β2–α1–γ2–β1–α2, which effectively illustrates the heterogeneity, with five different subunit types assembled into a single receptor molecule (Fig. 2g, Extended Data Fig. 6g and Supplementary Fig. 8). The last three subtypes were not found in dataset 2, probably owing to different limits of detection in the two sets of pooled samples, or differences among the sampled patient sets.

Both datasets revealed assemblies containing mixtures of β subunits. In dataset 2, the β2–α1–β2/3–α1–γ2 map shows β3 occupying a pentameric position typically held by β2, which may stem from the close similarity of β3 to β2, but not to β1 (Fig. 2h, Extended Data Fig. 6h and Supplementary Fig. 9). We also identified a mixed composition of β3–α1–γ2–β2/β3–α2 (Fig. 2i, Extended Data Fig. 6i and Supplementary Fig. 10), a stoichiometry that incorporates two β3 subunits. A third assembly from dataset 2, β2–α1–β1–α2–γ2, has the same stoichiometry as one found in dataset 1, but with γ2 and β1 subunits swapping positions (Fig. 2j, Extended Data Fig. 6j and Supplementary Fig. 11). All previously mentioned assemblies adhere to a common arrangement of two α subunits, two β subunits, and one γ subunit. However, the final composition in dataset 2 deviates from this pattern. The β2–α1–β1–β1–γ2 features a β1–β1 interface (Fig. 2k, Extended Data Fig. 6k and Supplementary Fig. 12). The existence of the β–β interface has been implicated in functional studies[35] and has also been observed in recombinant $GABA_A$ receptor structures, for instance β3–α4–β3–β3–γ2[5].

The 12 distinct receptor subunit assemblies stemming from 11 unique maps represent the diversity of native α1-containing $GABA_A$ receptors found in both the temporal and frontal lobes of the human brain, providing valuable insights into pharmacology. The β1–β1 subunit interface appears to be unique to human structures, contrasting with the study in mice. Furthermore, the presence of β3 in α1-receptor assemblies detected by cryo-EM suggests that this subunit in particular is present in higher amounts than in the mouse study, where it was only detected by mass spectrometry[8]. The structural distribution of $GABA_A$ receptor subunits generally corresponds to the findings of mass spectrometry (Fig. 1b). The presence of α4–6, γ1, γ3 and δ subunits in mass spectrometry, and its absence in the cryo-EM reconstructions, suggests they are indeed present in α1-containing receptors, but only in minor assemblies below our detection limit.

Insight into epilepsy drug mechanisms

While assigning subunits on the basis of model–map agreement, we noted strong density features at several subunit interfaces in the ECD, in locations analogous to those where benzodiazepines bind. In the most abundant and highest-resolution assembly of β2–α1–β2–α1–γ2, a shrimp-shaped density was found at the α1–γ2 benzodiazepine-binding site[36] (Fig. 3a). In two β3-containing assemblies (β2–α1–β2/3–α1–γ2 and β3–α1–γ2–β2/3–α1), the density in the α1–γ2 interface was similarly strong but elongated (Fig. 3b,c). We superimposed structures of several experimental $GABA_A$ receptor–drug complexes to determine whether these densities may correspond to locations of chemical groups of

known active compounds. We found that diazepam[37,38] and the negative modulator DMCM[39] partially fit this α1–γ2 density in the most abundant subunit assembly (Extended Data Fig. 8e,f), whereas DMCM better fits the elongated density at the α1–γ2 interface in the β2–α1–β2/3–α1–γ2 map (Extended Data Fig. 8g,h). The presence of these varied densities across the three compositions suggests that multiple types of ligands may bind at this site, with the density appearing as an average of several components.

Structural biology approaches have yet to reveal drug binding to an α–β interface, although modulators are suggested to bind at this site[40,41]. Here we observed density features suggestive of small-molecule binding (Extended Data Fig. 8a–c). Although the contributions of interfaces from these three compositions vary among the subunits (α2–β2, α1–β2/3 and α2–β3), the residues that pack around the densities are conserved and adopt similar conformations (Extended Data Fig. 8i). Together, the densities at α–β interfaces are distinct in size and shape, suggesting that these pockets exhibit pharmacological preferences. In contrast to the structurally undefined pharmacology at α–β interfaces, recombinant approaches have revealed histamine exerting agonist activity through the β3–β3 interface[5]. In the native structures, density at the β1–β1 interface in the β2–α1–β1–β1–γ2 composition is coordinated by the same set of residues as for histamine in the β3-containing receptor (Extended Data Fig. 8d,j).

The diverse densities detected in the native α1-containing $GABA_A$ receptors prompted us to consider potential candidates for ligands among the antiepileptic drugs taken by the patients, as well as endogenous neurosteroids and endozepines. Neurosteroids target the TMDs of $GABA_A$ receptors[42,43], which are far from the observed densities. The small-molecule endozepines are probably not present at sufficient physiological concentrations to exert substantial binding[44], and the diazepam binding inhibitor DBI[45,46] was not detected by mass spectrometry. Among the drugs taken by the 81 patients, six types were prevalent (Fig. 3d). These ligands act through multiple pathways[47], and were often taken in combination (Extended Data Tables 1 and 2). The two most common drugs, lacosamide (taken by 35 patients) and lamotrigine (taken by 28 patients), act principally by enhancing sodium channel inactivation. Levetiracetam (taken by 28 patients) targets synaptic vesicle 2A (SV2A) proteins. Zonisamide (taken by 16 patients) inhibits sodium and calcium channels and also potentiates inhibitory glycine receptors[48]. A total of 18 donors took carbamazepine or oxcarbazepine, which principally inhibit sodium channels but also positively modulate α1β2/3γ2 $GABA_A$ receptors[49,50]. The final category comprises benzodiazepines, including clobazam and clonazepam, which were taken by six patients, and are well defined positive modulators of $GABA_A$ receptors[51,52].

Next, we aimed to determine whether any of the prescribed drugs in the patient population might contribute to the density observed at native receptor subunit interfaces. We therefore tested the activity of the four most commonly prescribed drugs among the donors: lacosamide, lamotrigine, levetiracetam and zonisamide, which were not thought to affect $GABA_A$ receptors. We examined their modulatory effects on $GABA_A$ receptors at pharmacological concentrations[53] via patch clamp electrophysiology of transfected HEK cells. Lamotrigine and levetiracetam demonstrated small but significant potentiation of the α1β2γ2 receptor (Fig. 3e and Extended Data Fig. 8k,l), whereas lacosamide and zonisamide had no effect. To test whether the γ2 subunit was important for the activity of lamotrigine and levetiracetam, we tested modulation of GABA responses on the α1β2 $GABA_A$ receptor. These two drugs caused inhibition of the α1β2 $GABA_A$ isoform (Fig. 3e and Extended Data Fig. 8m,n). These findings raise the possibility that these commonly used antiepileptic drugs derive some of their efficacy from potentiating synaptic α1β2γ2 $GABA_A$ receptors. Furthermore, the switch from enhancement to inhibition suggests that the β2–β2 interface in the α1β2 receptor, which is absent in α1β2γ2, may contain the inhibitory site for these two drugs. Together, hints of potential drug occupancy in the native receptor structures led us to identify unexpected activities of classically prescribed antiepileptic drugs. We suggest that the densities in these interfaces represent a mixture of several compounds that indicate the potential of these sites for modulation. To more confidently map binding sites for levetiracetam and lamotrigine, we prepared cryo-EM samples of a recombinant α1β2γ2 receptor in the presence of the drugs. The results for levetiracetam were inconclusive, but we identified unambiguous density for lamotrigine at the α1–γ2 interface, in a position overlapping the binding site for benzodiazepines (Fig. 3f,g and Extended Data Fig. 9). Accordingly, this site may have a role in the therapeutic efficacy of lamotrigine in treating epilepsy.

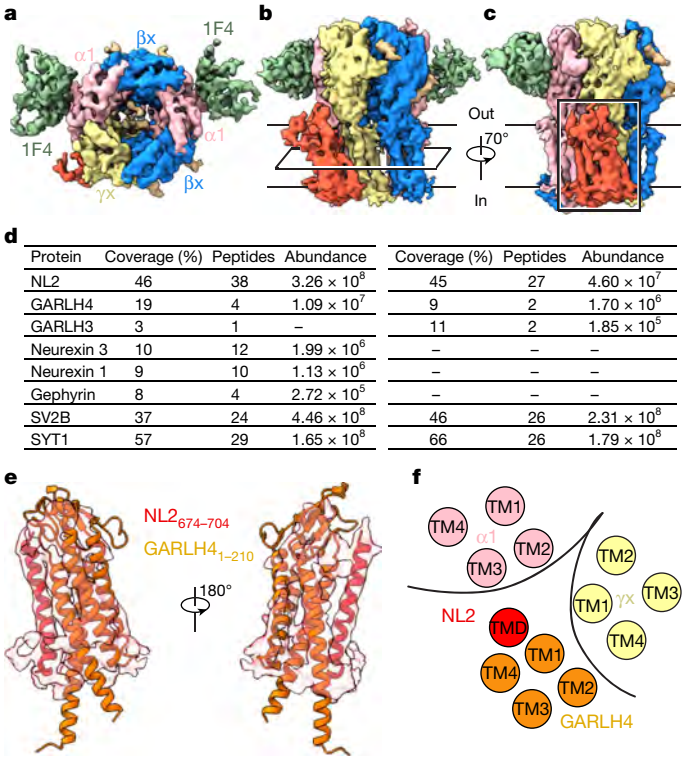

Fig. 4 | Proteins associated with native α1-containing $GABA_A$ receptors. **a**–**c**, Cryo-EM map of the $GABA_A$ receptor–TMD partner complex viewed from the extracellular side (**a**) and the plane of the membrane (**b**) and rotated by 70° in the plane of the membrane (**c**). The interaction partner density is shown in dark orange. **d**, Mass spectrometry of proteins associated with $GABA_A$ receptor isolated from brain tissue. Left, sample in detergent after affinity chromatography, from a pilot purification. Right, sample in lipid nanodiscs, from purification for structure determination. **e**, Interaction partner density map from **c** aligned with models of NL2 (residues 674–704, red) and GARLH4 (residues 41–210, orange). **f**, Cross-section schematic of suggested interactions between the α1 subunit, γx subunit, NL2 and GARLH4, based on **b**.

Identification of synaptic binding partners

Our first goal in studying native $GABA_A$ receptors was to define the major arrangements of subunits. To that end, we processed cryo-EM data with a focus on subunit-distinguishing features, which are mainly in the ECD. However, in parallel, we conducted classification based on differences in the TMD (Extended Data Fig. 4a). Unexpectedly, analysis of dataset 1 revealed a map featuring two 1F4 molecules bound to a receptor with five additional helical densities in the TMD. Subsequent refinement yielded a 4.1 Å resolution map (Fig. 4 and Extended Data Fig. 4b–d). Notably, the approximate five-fold symmetry of the pore was disrupted, probably because the nanodisc scaffold could not otherwise contain the whole receptor plus the additional interacting partner(s)

(Extended Data Fig. 4a). Distinctive N-glycosylation patterns along with 1F4 binding enabled us to assign the receptor composition as βx–α1–βx–α1–γx (Fig. 4a). Notably, the five unidentified helices, situated near the interface between the α1 and γ subunits, interact primarily with the TMD of the γ subunit (Fig. 4b,c).

The emergence of the new TMD density prompted us to revisit our mass spectrometry findings to aid in identifying these helices. In addition to the many $GABA_A$ receptor subunits, several proteins involved in $GABA_A$ receptor trafficking, clustering and anchoring co-purified with the receptor (Fig. 4d and Extended Data Fig. 1a,c). A subset of these associate directly with $GABA_A$ receptors. For instance, NL2 and the GARLH family—specifically GARLH4—form complexes with $GABA_A$ receptors through the TMD of γ subunits[23,54]. NL2 is a single-pass transmembrane protein, whereas GARLH4 has four transmembrane helices. Gephyrin helps cluster the receptors but is a soluble protein that interacts with the intracellular loop of the receptor. Neurexins modulate GABA-dependent synaptic responses by associating with postsynaptic $GABA_A$ receptors[18] by reaching across from the presynaptic side. There is no evidence for direct interactions of SV2B and SYT1 with $GABA_A$ receptors, and these proteins are mainly presynaptic. The mostly likely binding partners of the $GABA_A$ TMD among the co-purified proteins are GARLH4 and NL2.

We rigid-body-fitted the AlphaFold2-predicted[55] TMDs of NL2 (residues 674–704) and GARLH4 (residues 1–210), in conjunction with the model of the β2–α1–β2–α1–γ2 $GABA_A$ receptor, into the density map (Fig. 4e). The combination of NL2 and GARLH4 fit well into the density without needing local refinement. The fitting is consistent with previous functional studies suggesting that GARLH4 bridges the connection between NL2 and the TMD of the γ subunit[23] (Fig. 4f). The spatial arrangement of helices within GARLH4 matches those in an experimental structure of LHFPL5 (a homologue of GARLH4), and the site of NL2 binding is similar to a bound helical partner of LHFPL5[56]. Our findings thus provide a view into probable synaptic interactions of NL2 and GARLH4 with native α1-containing $GABA_A$ receptors. However, further validation and investigation are required to resolve a well-ordered complex structure, as side-chain densities remain unclear.

Discussion

Previous structural investigations have enabled a good understanding of the composition of $GABA_A$ receptors and how drugs act on them. Recombinant studies on major synaptic and extrasynaptic receptor subtypes have revealed details at high resolution about several subunit assemblies[4–7]. However, they have not directly addressed whether these assemblies are present physiologically or whether they are abundant or minor components in brain tissue. A study on structures of native $GABA_A$ receptors from mouse brain mapped three abundant subunit compositions and uncovered the presence of a native neurosteroid modulator[8]. Although this was a critical step for the field, this approach is inherently limited for making inferences about the human brain. The complexity in physiological assemblies was already thought to be greater in human brains compared with mouse[15,16], and was used to explain failures in therapeutic development when translating results from mouse to human[57]. Our study on human brain tissue directly addresses the composition of the major subunit assemblies in the temporal and frontal lobes. Our structures identified unexpected drug activities and probable interactions with synaptic proteins. However, human brain tissue is an exceptionally precious resource, and very small amounts are available from individual surgeries, precluding comparisons between individuals that could inform on disease mechanisms. There are also regional limitations when obtaining human brain tissue from surgery—for example, drug-resistant temporal lobe epilepsy is relatively commonly treated with resection, so a large proportion of the available tissue is from the temporal lobe. Furthermore, interpretation is complicated by the unknown effects of drug regimens on subunit expression and individual genetic variants, although we found no evidence of mutations when analysing the structural data. The increasing prevalence of non-resective epilepsy treatments, such as laser interstitial thermal therapy and responsive neurostimulator implants, also means that access to neurosurgical specimens is likely to decrease further in the future. Nonetheless, by pooling tissue from the diverse population of patients, we have been able to survey the most abundant human receptor assemblies, which were common to both datasets.

Multiple sources of variation may explain the difference in the minor structural assemblies found in the two datasets, including patient sex, age, duration of epilepsy, site of resection and drug regimen. Dataset 2 includes a higher percentage of males (72%) than dataset 1 (51%) and higher levels of some $GABA_A$ subunits are found in male versus female temporal cortex; by contrast, we did not find age-related differences in the relatively young patient population that we surveyed[58,59]. Comparisons between tissue from epilepsy surgeries outside the epileptogenic zone and healthy tissue removed during brain tumour surgeries suggest that when pooled from a given patient, these tissues are not significantly different in $GABA_A$ receptor subunit levels[60]. This finding suggests that the presence of the disease and variations related to the disease (including duration) are likely to have a minimal impact on our results. The resection sites were balanced between our two datasets, with around 90% of resections in both datasets coming from the temporal lobe. Mouse studies indicate that chronic treatment with epilepsy drugs, specifically benzodiazepines, can indeed affect $GABA_A$ subunit levels[61]. Five patients in dataset 1 were chronically prescribed benzodiazepines, versus one patient in dataset 2 (Extended Data Tables 1 and 2). Mouse studies suggest that these drugs can trigger a decrease in the amounts of α1, β2, α3 and δ subunits; differences in subunit assemblies between the two datasets are not in line with a benzodiazepine effect, probably because only a small fraction of the patients was prescribed this specific drug class. Overall, we cannot confidently attribute the differences in subunit compositions between the two datasets to variations in patient demographics or conditions—these differences are likely to be because of the detection limits of cryo-EM for minor species, along with other undefined variations within the patient pools.

Understanding $GABA_A$ signalling in the brain requires knowledge of the explicit receptor subunit arrangements. Different subunits and interfaces between them tune pharmacology and channel biophysics. There are many other essential pieces of the signalling puzzle, including spatial and cellular distributions of specific subunit assemblies. However, as a starting point, we need to know the extent of heterogeneity in subunit compositions. Here we addressed this question by purifying receptors from human tissue. We studied the population of receptors containing the α1 subunit, as this subunit appears to be the most promiscuous with respect to its subunit partners. We identified the predominant assembly in the human temporal lobe as β2–α1–β2–α1–γ2. Assemblies with heterogeneous compositions were also abundant. The α1, α2, α3 and β1, β2, β3 and γ2 positions can swap with each other and assemble in multiple ratios, giving rise to single receptors that contain five different subunits, as well as receptors with a β–β interface. The implications for pharmacology are diverse. For example, drugs deemed or engineered to be specific for α2-containing receptors are likely to also bind to receptors that contain an α1 subunit. Although the complexity is daunting, it serves as a basis for developing tools to target the now explicitly defined native interfaces. Our results also identify previously unknown interactions with epilepsy drugs and interactions with additional proteins. Mass spectrometry and features in the experimental map identify NL2 and GARLH4, proteins that have been shown to interact with the receptor in mouse cerebellum[17], as probable binding partners. Together, our findings illustrate the complexity of $GABA_A$ receptor subunit assemblies and their interactions with other proteins in the human brain.

Online content

Any methods, additional references, Nature Portfolio reporting summaries, source data, extended data, supplementary information, acknowledgements, peer review information; details of author contributions and competing interests; and statements of data and code availability are available at https://doi.org/10.1038/s41586-024-08454-1.

1. Olsen, R. W. & Sieghart, W. International Union of Pharmacology. LXX. Subtypes of γ-aminobutyric acid$_A$ receptors: classification on the basis of subunit composition, pharmacology, and function. Update. *Pharmacol. Rev.* **60**, 243–260 (2008).
2. Sieghart, W. & Savic, M. M. International Union of Basic and Clinical Pharmacology. CVI: GABA$_A$ receptor subtype- and function-selective ligands: key issues in translation to humans. *Pharmacol. Rev.* **70**, 836–878 (2018).
3. Olsen, R. W. & Sieghart, W. GABA$_A$ receptors: subtypes provide diversity of function and pharmacology. *Neuropharmacology* **56**, 141–148 (2009).
4. Kim, J. J. & Hibbs, R. E. Direct structural insights into GABA$_A$ receptor pharmacology. *Trends Biochem. Sci.* **46**, 502–517 (2021).
5. Sente, A. et al. Differential assembly diversifies GABA$_A$ receptor structures and signalling. *Nature* **604**, 190–194 (2022).
6. Kasaragod, V. B. et al. The molecular basis of drug selectivity for alpha5 subunit-containing GABA$_A$ receptors. *Nat. Struct. Mol. Biol.* **30**, 1936–1946 (2023).
7. Cowgill, J. et al. Structure and dynamics of differential ligand binding in the human rho-type GABA$_A$ receptor. *Neuron* **111**, 3450–3464.e3455 (2023).
8. Sun, C., Zhu, H., Clark, S. & Gouaux, E. Cryo-EM structures reveal native GABA$_A$ receptor assemblies and pharmacology. *Nature* **622**, 195–201 (2023).
9. Nutt, D. GABA$_A$ receptors: subtypes, regional distribution, and function. *J. Clin. Sleep Med.* **2**, S7–S11 (2006).
10. Chuang, S. H. & Reddy, D. S. Genetic and molecular regulation of extrasynaptic GABA$_A$ receptors in the brain: therapeutic insights for epilepsy. *J. Pharmacol. Exp. Ther.* **364**, 180–197 (2018).
11. Sigel, E. & Steinmann, M. E. Structure, function, and modulation of GABA$_A$ receptors. *J. Biol. Chem.* **287**, 40224–40231 (2012).
12. Mihic, S. J. & Harris, R. A. GABA and the GABA$_A$ receptor. *Alcohol Health Res, World* **21**, 127–131 (1997).
13. Pirker, S., Schwarzer, C., Wieselthaler, A., Sieghart, W. & Sperk, G. GABA$_A$ receptors: immunocytochemical distribution of 13 subunits in the adult rat brain. *Neuroscience* **101**, 815–850 (2000).
14. Loup, F. et al. A highly sensitive immunofluorescence procedure for analyzing the subcellular distribution of GABAA receptor subunits in the human brain. *J. Histochem. Cytochem.* **46**, 1129–1139 (1998).
15. Sperk, G. et al. Immunohistochemical distribution of 10 GABA$_A$ receptor subunits in the forebrain of the rhesus monkey *Macaca mulatta*. *J. Comp. Neurol.* **528**, 2551–2568 (2020).
16. Stefanits, H. et al. GABA$_A$ receptor subunits in the human amygdala and hippocampus: Immunohistochemical distribution of 7 subunits. *J. Comp. Neurol.* **526**, 324–348 (2018).
17. Martenson, J. S., Yamasaki, T., Chaudhury, N. H., Albrecht, C. & Tomita, S. Assembly rules for GABA$_A$ receptor complexes in the brain. *eLife* **6**, e27443 (2017).
18. Zhang, C. et al. Neurexins physically and functionally interact with GABA$_A$ receptors. *Neuron* **66**, 403–416 (2010).
19. Liu, Y. T. et al. Mesophasic organization of GABA$_A$ receptors in hippocampal inhibitory synapses. *Nat. Neurosci.* **23**, 1589–1596 (2020).
20. Tretter, V. et al. Gephyrin, the enigmatic organizer at GABAergic synapses. *Front. Cell Neurosci.* **6**, 23 (2012).
21. Spencer, D. & Burchiel, K. Selective amygdalohippocampectomy. *Epilepsy Res. Treat.* **2012**, 382095 (2012).
22. Zhu, S. et al. Structure of a human synaptic GABA$_A$ receptor. *Nature* **559**, 67–72 (2018).
23. Yamasaki, T., Hoyos-Ramirez, E., Martenson, J. S., Morimoto-Tomita, M. & Tomita, S. GARLH family proteins stabilize GABA$_A$ receptors at synapses. *Neuron* **93**, 1138–1152.e1136 (2017).
24. Bencsits, E., Ebert, V., Tretter, V. & Sieghart, W. A significant part of native γ-aminobutyric acid$_A$ receptors containing α4 subunits do not contain γ or δ subunits. *J. Biol. Chem.* **274**, 19613–19616 (1999).
25. Benke, D. et al. Analysis of the presence and abundance of GABA$_A$ receptors containing two different types of α subunits in murine brain using point-mutated α subunits. *J. Biol. Chem.* **279**, 43654–43660 (2004).
26. Mertens, S., Benke, D. & Mohler, H. GABA$_A$ receptor populations with novel subunit combinations and drug binding profiles identified in brain by α5- and δ-subunit-specific immunopurification. *J. Biol. Chem.* **268**, 5965–5973 (1993).
27. Scholze, P. et al. Two distinct populations of α1α6-containing GABAA-receptors in rat cerebellum. *Front. Synaptic Neurosci.* **12**, 591129 (2020).
28. Zhang, S. et al. One-step construction of circularized nanodiscs using SpyCatcher–SpyTag. *Nat. Commun.* **12**, 5451 (2021).
29. Dalal, V. et al. Lipid nanodisc scaffold and size alter the structure of a pentameric ligand-gated ion channel. *Nat. Commun.* **15**, 25 (2024).
30. Engin, E., Liu, J. & Rudolph, U. alpha2-containing GABA$_A$ receptors: a target for the development of novel treatment strategies for CNS disorders. *Pharmacol. Ther.* **136**, 142–152 (2012).
31. Nguyen, Q. A. & Nicoll, R. A. The GABA$_A$ receptor β subunit is required for inhibitory transmission. *Neuron* **98**, 718–725 e713 (2018).
32. Jensen, M. L. et al. The β subunit determines the ion selectivity of the GABA$_A$ receptor. *J. Biol. Chem.* **277**, 41438–41447 (2002).
33. Uygun, D. S. et al. Knockdown of GABA$_A$ α3 subunits on thalamic reticular neurons enhances deep sleep in mice. *Nat. Commun.* **13**, 2246 (2022).
34. Dias, R. et al. Evidence for a significant role of α3-containing GABA$_A$ receptors in mediating the anxiolytic effects of benzodiazepines. *J. Neurosci.* **25**, 10682–10688 (2005).
35. Saras, A. et al. Histamine action on vertebrate GABA$_A$ receptors: direct channel gating and potentiation of GABA responses. *J. Biol. Chem.* **283**, 10470–10475 (2008).
36. Sigel, E. & Ernst, M. The benzodiazepine binding sites of GABA$_A$ receptors. *Trends Pharmacol. Sci.* **39**, 659–671 (2018).
37. Kim, J. J. et al. Shared structural mechanisms of general anaesthetics and benzodiazepines. *Nature* **585**, 303–308 (2020).
38. Masiulis, S. et al. GABA$_A$ receptor signalling mechanisms revealed by structural pharmacology. *Nature* **565**, 454–459 (2019).
39. Zhu, S. et al. Structural and dynamic mechanisms of GABA$_A$ receptor modulators with opposing activities. *Nat. Commun.* **13**, 4582 (2022).
40. Ramerstorfer, J. et al. The GABA$_A$ receptor α+β− interface: a novel target for subtype selective drugs. *J. Neurosci.* **31**, 870–877 (2011).
41. Varagic, Z. et al. Identification of novel positive allosteric modulators and null modulators at the GABA$_A$ receptor α+β− interface. *Br. J. Pharmacol.* **169**, 371–383 (2013).
42. Mortensen, M. et al Forty Years searching for neurosteroid binding sites on GABA$_A$ receptors. *Neuroscience* https://doi.org/10.1016/j.neuroscience.2024.06.002 (2024).
43. Legesse, D. H. et al. Structural insights into opposing actions of neurosteroids on GABA$_A$ receptors. *Nat. Commun.* **14**, 5091 (2023).
44. Tonon, M. C. et al. Endozepines and their receptors: structure, functions and pathophysiological significance. *Pharmacol. Ther.* **208**, 107386 (2020).
45. Bormann, J. Electrophysiological characterization of diazepam binding inhibitor (DBI) on GABA$_A$ receptors. *Neuropharmacology* **30**, 1387–1389 (1991).
46. Everlien, I. et al. Diazepam binding inhibitor governs neurogenesis of excitatory and inhibitory neurons during embryonic development via GABA signaling. *Neuron* **110**, 3139–3153.e3136 (2022).
47. Sanchez, J. D., Gomez-Carpintero, J., Gonzalez, J. F. & Menendez, J. C. Twenty-first century antiepileptic drugs. An overview of their targets and synthetic approaches. *Eur. J. Med. Chem.* **272**, 116476 (2024).
48. Devenish, S. O. et al. The anticonvulsant zonisamide positively modulates recombinant and native glycine receptors at clinically relevant concentrations. *Neuropharmacology* **182**, 108371 (2021).
49. Liu, L. et al. The mechanism of carbamazepine aggravation of absence seizures. *J. Pharmacol. Exp. Ther.* **319**, 790–798 (2006).
50. Zheng, T. et al. Oxcarbazepine, not its active metabolite, potentiates GABA$_A$ activation and aggravates absence seizures. *Epilepsia* **50**, 83–87 (2009).
51. Hammer, H., Ebert, B., Jensen, H. S. & Jensen, A. A. Functional characterization of the 1,5-benzodiazepine clobazam and its major active metabolite *N*-desmethylclobazam at human GABA$_A$ receptors expressed in *Xenopus laevis* oocytes. *PLoS ONE* **10**, e0120239 (2015).
52. Gauthier, A. C. & Mattson, R. H. Clobazam: a safe, efficacious, and newly rediscovered therapeutic for epilepsy. *CNS Neurosci. Ther.* **21**, 543–548 (2015).
53. Reimers, A. et al. Reference ranges for antiepileptic drugs revisited: a practical approach to establish national guidelines. *Drug Des. Dev. Ther.* **12**, 271–280 (2018).
54. Tomita, S. Molecular constituents and localization of the ionotropic GABA receptor complex in vivo. *Curr. Opin. Neurobiol.* **57**, 81–86 (2019).
55. Jumper, J. et al. Highly accurate protein structure prediction with AlphaFold. *Nature* **596**, 583–589 (2021).
56. Ge, J. et al. Structure of mouse protocadherin 15 of the stereocilia tip link in complex with LHFPL5. *eLife* **7**, e38770 (2018).
57. Skolnick, P. Anxioselective anxiolytics: on a quest for the Holy Grail. *Trends Pharmacol. Sci.* **33**, 611–620 (2012).
58. Pandya, M. et al. Sex- and age-related changes in GABA signaling components in the human cortex. *Biol. Sex Differ.* **10**, 5 (2019).
59. Ethiraj, J. et al. The effect of age and sex on the expression of GABA signaling components in the human hippocampus and entorhinal cortex. *Sci Rep.* **11**, 21470 (2021).
60. Chameh, H. M. et al. Distinctive biophysical features of human cell-types: insights from studies of neurosurgically resected brain tissue. *Front. Synaptic Neurosci.* **15**, 1250834 (2023).
61. Engin, E. GABA$_A$ receptor subtypes and benzodiazepine use, misuse, and abuse. *Front. Psychiatry* **13**, 1060949 (2022).

Publisher's note Springer Nature remains neutral with regard to jurisdictional claims in published maps and institutional affiliations.

Springer Nature or its licensor (e.g. a society or other partner) holds exclusive rights to this article under a publishing agreement with the author(s) or other rightsholder(s); author self-archiving of the accepted manuscript version of this article is solely governed by the terms of such publishing agreement and applicable law.

© The Author(s), under exclusive licence to Springer Nature Limited 2025

Methods

Human tissue

The study included 81 patients with temporal and frontal lobe epilepsy, 20 to 70 years of age, who were undergoing surgical resection as part of their treatment plan for medication-resistant epilepsy. Participants came from the University of Texas Southwestern (UTSW) epilepsy surgery programme across a time span of seven years. The protocol was approved by the UTSW Institutional Review Board on Human Subjects Research prior to data collection, and all participants provided informed written consent. After resection, the brain samples were rinsed with cold PBS and any tissue damaged by electrocautery was dissected away and discarded. The tissue was then divided into cryo-tubes and flash frozen in liquid nitrogen. All tissue processing was completed on ice within an hour of resection, typically within 20 min. Participant information is summarized in Extended Data Tables 1 and 2.

Fab 1F4 expression and purification

The coding sequence of Fab 1F4, which recognizes the human $GABA_A$ receptor α1 subunit, was determined previously[22]. DNA fragments encoding the heavy and light chains were synthesized and subcloned into the pCEP4 mammalian expression vector (Invitrogen). A signal peptide from mouse IgG (MGWSCIILFLVATATGVHS) was added to the 5′ ends of both genes in place of the original signal peptides to boost expression. To facilitate affinity purification, 3×Flag and 8×His tags were added to the C terminus of the heavy chain. Recombinant Fab expression was carried out using the ExpiCHO expression system (Thermo Fisher) by transient transfection. Four-hundred millilitres of ExpiCHO cells were transfected with 0.4 mg total plasmid DNA at a cell density of 7 million per ml at 37 °C, 8% CO_2. Cells were collected after 9 days by centrifugation for 20 min at 6,000*g*. The supernatant was filtered (0.22 μm) and concentrated using a 30 kDa cutoff Vivaflow 200 (Sartorius) after adjusting pH to 8.0. Fab 1F4 was purified using a 5 ml HisTrap HP column (Cytiva) with binding buffer (50 mM Tris-HCl, pH 8.0, 200 mM NaCl, 20 mM imidazole, pH 8.0) and elution buffer (20 mM Tris-HCl, pH 8.0, 200 mM NaCl, 500 mM imidazole, pH 8.0). The eluted fractions were pooled for concentration and gel filtration assay after analysis by SDS–PAGE. The collected fractions (~30 mg) were stored at −80 °C for future use.

Native α1-containing $GABA_A$ receptor purification

Purifications were performed from two sets of pooled samples; samples from 45 patients led to dataset 1, and samples from 36 patients led to dataset 2. For purification, the brain tissue was washed 3 times in ice-cold 1× PBS (pH 7.4) by centrifugation for 10 min at 6,000*g* followed by resuspension. The final pellet was resuspended in ice-cold buffer A (20 mM Tris-HCl, pH 7.4, 200 mM NaCl, 2 mM GABA) supplemented with 0.2 mM phenylmethyl sulfonyl fluoride (PMSF, Sigma-Aldrich). The suspension was processed with a Dounce homogenizer and further disrupted using an Avestin Emulsiflex. This homogenate was centrifuged at 10,000*g* for 20 min, and the supernatant was further centrifuged at 186,000*g* for 2 h to pellet the membrane. The membrane pellet was collected, then mechanically homogenized and solubilized with buffer A containing 1% (w/v) lauryl maltose neopentyl glycol (LMNG; Anatrace) and protease inhibitors (aprotinin, leupeptin, pepstatin A and PMSF) for 3 h. The membrane solubilization and subsequent affinity chromatography were carried out at 4 °C. Next, the mixture was clarified by centrifugation at 186,000*g* for 1 h. Fab 1F4 was added to the supernatant (6 mg for 45-patient sample; 4 mg for 36-patient sample), and incubated for 2.5 h. Then, pre-equilibrated M2 anti-Flag resin (Sigma-Aldrich) was added to bind the Fab 1F4 and native α1-containing $GABA_A$ receptors for 3.5 h while rotating. The resin was washed with 5 column volumes buffer A supplemented with protease inhibitors, 0.01% (w/v) LMNG, and 0.01% (w/v) brain polar lipids (Avanti).

Receptor–nanodisc reconstitution

The on-bead nanodisc reconstitution was performed with the spMSP1D1 scaffold protein (a gift from H. Bao, Addgene #172482)[28] and brain polar lipids. $GABA_A$ receptor-bound Flag resin was resuspended with buffer A containing 0.01% (w/v) LMNG and 0.01% (w/v) brain polar lipids and incubated for 30 min at 4 °C. Then, spMSP1D1 was added and incubated for another 30 min at 4 °C. The molar ratio of receptor, lipids and spMSP1D1 was 1:100:10. Detergent was removed by adding Bio-Beads SM2 (Bio-Rad) to a final concentration of 60 mg ml^{-1} while rotating overnight at 4 °C. The next day, excess lipids and spMSP1D1 were removed by washing with buffer A. Next, the Fab 1F4-bound receptors were eluted with buffer A containing 0.15 mg ml^{-1} 3× Flag peptide (Sigma-Aldrich). The eluted fractions were concentrated and run over a Superose 6 Increase 10/300 GL column (Cytiva). For just the 36-patient sample, two separate purifications were performed after isolating membranes, to test two different crosslinking reagents. In these cases, after affinity chromatography, the eluted protein was incubated with either 5 mM glutaraldehyde, or 5 mM Bs3 crosslinking agent (both from Sigma-Aldrich) for 2 h prior to preparative SEC. The peak fractions were analysed by SDS–PAGE, then collected and concentrated to an absorbance at 280 nm (A_{280}) of 6.4 for the 45-patient dataset (dataset 1) and 1.4 for the 36-patient dataset (dataset 2).

Cryo-EM sample preparation and data collection

Cryo-EM grids were prepared using a Vitrobot Mark IV (FEI). 300-mesh copper R1.2/1.3 holey carbon grids (Quantifoil) were used for dataset 1. Three-hundred mesh copper R 2/1 overlaid with 2-nm continuous carbon grids (Quantifoil) were used for dataset 2. Before freezing grids, 0.5 mM fluorinated Fos-Choline-8 (Anatrace) was mixed with the protein sample to induce random particle orientations. Three microlitres of sample was applied to glow-discharged grids and blotted for 3.5 s at 4 °C with 100% humidity, and then plunge-frozen in liquid ethane. Electron microscopy images were collected at the University of California San Diego (UCSD) Cryo-EM Facility on the Titan Krios G4 (Thermo Fisher Scientific) at 300 keV equipped with a Gatan BioContinuum energy filter. The total exposure was 50 $e^- Å^{-2}$ and the defocus range was set to −2.2 μm to −1.0 μm. Details for both datasets are provided in Extended Data Table 3.

Cryo-EM data processing

Both datasets were processed using a CryoSPARC 4.4[62] workflow. First, the images were motion and gain corrected using patch motion correction. Contrast transfer function estimation was performed with Patch CTF. For each dataset, particles were subjected to 3 rounds of 2D classification to remove junk particles. The good 2D classes were selected to generate ab initio models with four seeds, followed by two rounds of heterogenous refinement with junk volumes to further remove bad particles. The retained particles were re-extracted at full size and aligned with non-uniform refinement. The consensus maps were obtained at 2.6 Å (dataset 1) and 2.8 Å (dataset 2). To resolve the heterogeneity of native $GABA_A$ receptors, two kinds of strategies, both using focused (masked) 3D classification without alignment were applied, described below. In processing of dataset 2, we found no differences between the two crosslinking agents mentioned above, so images were combined from both samples.

Dataset 1 processing

The first classification approach was focused on resolving distinct $GABA_A$ receptor subunit assemblies. Focused 3D classification with an ECD mask was carried out to separate classes with one Fab versus two Fabs bound. Then, particles from 3D classes with two Fabs, or one Fab, were pooled with each other; these particle sets were aligned in 3D using non-uniform refinement. For the two-Fab particles, further focused 3D classification was used to identify the heterogeneity but no

indications of mixtures of subunits at any positions were found in the composition of β2–α1–β2–α1–γ2. For the one-Fab particles, focused 3D classification was carried out and followed by non-uniform refinements. The processing workflow is shown in Extended Data Fig. 2. Chain IDs are always represented in an anticlockwise order as follows: βx (chain A)–α1 (chain B)–X (chain C)–X (chain D)–X (chain E) (Supplementary Figs. 1–11). Five types of masks were tested in the secondary 3D classification: a mask focused on chain B; a mask focused on chain D; a mask focused on chain A and B; a mask focused on chain C, D and E; and a mask focused on chain D and E. All the masks were generated with UCSF ChimeraX (1.7.1)[63]. The focused 3D classification with the mask on chain A and chain B was the most effective in separating particles. This masked classification was followed by further focused 3D classifications, from which six compositions were revealed including: β2–α1–γ2–β2–α2, β2/3–α1–β2–α2–γ2, β2–α1–β2–α2–γ2, β2–α1–β2/3–α2–γ2, β2–α1–β2–α2/3–γ2 and β2–α1–γ2–β1–α2.

The second classification approach was designed to investigate interesting possibilities in the TMD of $GABA_A$ receptors, including compositional or conformational heterogeneity and interacting proteins. Two rounds of focused 3D classification with a TMD mask, followed by non-uniform refinements, were performed (Extended Data Fig. 4). After the first focused 3D classification, one class with a poorly ordered TMD was identified. Ultimately, density indicative of five transmembrane helices in addition to the TMD of the $GABA_A$ receptor was discovered. Through docking of likely candidates identified in mass spectrometry, GARLH4 and NL2 are the suggested bound proteins.

Dataset 2 processing

Focused 3D classification with an ECD mask was also applied to resolve distinct $GABA_A$ receptor subunit assemblies. Then, 3D classes with two Fabs and those with one Fab, were pooled with each other; these particle sets were aligned in 3D using non-uniform refinement (Extended Data Fig. 3). For the two-Fab particles, further focused 3D classification was used to resolve heterogeneity, and a total of two compositions including β2–α1–β2–α1–γ2 and β2–α1–β2/3–α1–γ2 were identified. For the one-Fab particles, focused 3D classification with a mask on chains A and B was carried out and followed by non-uniform refinements. Classification and refinement of the one-Fab particles yielded five subunit assemblies: β2–α1–γ2–β2–α2, β2/3–α1–β2–α2–γ2, β2–α1–β1–α2–γ2, β3–α1–γ2–β2/3–α2 and β2–α1–β1–β1–γ2.

From both datasets, we observed three common compositions: β2–α1–β2–α1–γ2, β2–α1–γ2–β2–α2 and β2/3–α1–β2–α2–γ2. Particles for these compositions, from the two datasets were combined and non-uniform refinement was performed to generate the final maps for these three compositions. For these 3 abundant assemblies, additional processing was performed to further improve map quality, related to a common feature observed in $GABA_A$ receptors, a disordered TMD of the γ subunit. Focused 3D classification without alignment on the entire TMD was performed (Extended Data Fig. 5), as there were sufficient particles available after combining these particle sets. Particles with a five-fold symmetric TMD were selected for non-uniform refinement. The overall resolution for all maps was estimated using the gold-standard Fourier shell correlation 0.143 criterion.

Model building, refinement and validation

A four-step procedure was developed to identify and assign the $GABA_A$ receptor subunits in the maps. First, the subunit bound by Fab 1F4 is assigned as α1. Second, identification is based on the N-linked glycosylation patterns of the subunits, such as the hallmark glycosylation site in the Cys-loop unique to β subunits. Third, subunits involved in GABA binding are identified as α and β subunits on the basis of their binding interfaces. Finally, the side-chain density is checked after docking the target subunit models. A total of 11 distinct maps were obtained from these two datasets. Five of these maps contain a currently unresolvable mixture of two subunits at a single position. The full set of maps includes: β2–α1–β2–α1–γ2 (Supplementary Fig. 2), β2–α1–γ2–β2–α2 (Supplementary Fig. 3), β2/3–α1–β2–α2–γ2 (Supplementary Fig. 4), β2–α1–β2–α2–γ2 (Supplementary Fig. 5), β2–α1–β2/3–α2–γ2 (Supplementary Fig. 6), β2–α1–β2–α2/3–γ2 (Supplementary Fig. 7), β2–α1–γ2–β1–α2 (Supplementary Fig. 8), β2–α1–β2/3–α1–γ2 (Supplementary Fig. 9), β3–α1–γ2–β2/3–α2 (Supplementary Fig. 10), β2–α1–β1–α2–γ2 (Supplementary Fig. 11) and β2–α1–β1–β1–γ2 (Supplementary Fig. 12). All the details used in subunit assignment are listed in the supplementary figures.

For model building and refinement of β2–α1–β2–α1–γ2, the recombinant β2–α1–β2–α1–γ2 with Fab 1F4 bound (Protein Data Bank (PDB): 6X3T) and β3–α1–β3–α1–γ2 (PDB: 6I53) were used as the initial models after docking into the map using UCSF ChimeraX. The refined model of β2–α1–β2–α1–γ2 was used as the initial model for the additional 11 models. The map with the composition of β3–α1–γ2–β2/3–α2 was used to build two models: β3–α1–γ2–β2–α2 and β3–α1–γ2–β3–α2. The models underwent a series of iterative adjustments manually in Coot (v.9.8.92)[64], followed by Phenix (1.20.1) real space refinement[65] with secondary structure restraints. The density for the γ-TMD was too poor to model that domain of the subunit in the following assemblies: β2–α1–β2–α2–γ2, β2–α1–β2/3–α2–γ2, β2–α1–β2–α2/3–γ2, β2–α1–γ2–β1–α2, β2–α1–β2/3–α1–γ2, β3–α1–γ2–β2/3–α1 and β2–α1–β1–α2–γ2; accordingly, in these cases, the TMD of the γ2 subunit was not modeled. Models were validated using MolProbity v4.5[66]. The validation statistics of the PDB models are provided in Extended Data Tables 4 and 5. Subunit interface densities in Fig. 3 and Extended Data Fig. 8 are shown at the following thresholds, rendered using ChimeraX: Fig. 3a, 0.14; Fig. 3b, 0.14; Fig. 3c, 0.14; Extended Data Fig. 8a, 0.15; Extended Data Fig. 8b, 0.21; Extended Data Fig. 8c, 0.12; Extended Data Fig. 8d,j, 0.11; Extended Data Fig. 8e,f, 0.14; Extended Data Fig. 8g,h, 0.14. The pore diameter was calculated by HOLE v.2[67] and rendered using PyMOL (v.2.5.5, Schrodinger).

Mass spectrometry

Proteins were identified after SDS–PAGE separation by mass spectrometry using standard methods[68]. Proteins from dataset 1 were analysed at the UT Southwestern proteomics facility, and proteins from the dataset 2 at the UCSD proteomics core. The dataset 1 samples were digested overnight with trypsin (Pierce) following reduction and alkylation with dithiothreitol and iodoacetamide (Sigma-Aldrich). The samples then underwent solid-phase extraction cleanup with an Oasis HLB plate (Waters) and the resulting samples were injected onto either a Q Exactive HF or Orbitrap Fusion Lumos mass spectrometer coupled to an Ultimate 3000 RSLC-Nano liquid chromatography system. Samples were injected onto a 75-μm internal diameter, 15-cm-long EasySpray column (Thermo) for Q Exactive HF samples or a 75-μm internal diameter, 75-cm long EasySpray column (Thermo) for Orbitrap Fusion Lumos samples and eluted with a gradient from 0–28% buffer B over 90 min. Buffer A contained 2% (v/v) acetonitrile (ACN) and 0.1% formic acid in water, and buffer B contained 80% (v/v) ACN, 10% (v/v) trifluoroethanol, and 0.1% formic acid in water. The mass spectrometer was operated in positive ion mode with a source voltage of 2.5 kV (Q Exactive HF) or 2.2 kV (Orbitrap Fusion Lumos) and an ion transfer tube temperature of 275 °C. MS scans were acquired at 120,000 resolution in the Orbitrap. For Q Exactive HF samples, up to 20 tandem mass spectrometry (MS/MS) spectra were obtained in the ion trap for each full spectrum acquired using higher-energy collisional dissociation (HCD) for ions with charges 2–8. For Orbitrap Fusion Lumos samples, up to 10 MS/MS spectra were obtained in the ion trap for each full spectrum acquired using higher-energy collisional dissociation (HCD) for ions with charges 2–7. Dynamic exclusion was set for either 20 s (Q Exactive HF) or 25 s (Orbitrap Fusion Lumos) after an ion was selected for fragmentation. Raw MS data files were analysed using Proteome Discoverer v. 3.0 (Thermo), with peptide identification performed using a tryptic search with Sequest HT against the human reviewed protein

database from UniProt. Fragment and precursor tolerances of 10 ppm and either 0.02 Da (Q Exactive HF) or 0.6 Da (Orbitrap Fusion Lumos) were specified, and three missed cleavages were allowed. Carbamidomethylation of Cys was set as a fixed modification, with oxidation of Met set as a variable modification. The false-discovery rate (FDR) cutoff was 1% for all peptides.

The mass spectrometry results from dataset 2 were obtained using the following method. The gel slices were cut to 1 mm × 1 mm cubes and destained 3 times by first washing with 100 µl of 100 mM ammonium bicarbonate for 15 min, followed by addition of the same volume of ACN for 15 min. The samples were dried, then reduced by mixing with 200 µl of 100 mM ammonium bicarbonate and 10 mM dithiothreitol and incubated at 56 °C for 30 min. The liquid was removed and 200 µl of 100 mM ammonium bicarbonate, 55 mM iodoacetamide was added to the gel pieces and incubated at room temperature in the dark for 20 min. Gels were washed with 100 mM ammonium bicarbonate for 15 min, then the same volume of ACN was added to dehydrate the gel pieces. The solution was then removed and samples were dried. For digestion, ice-cold trypsin (0.01 µg µl^{-1}) in 50 mM ammonium bicarbonate was added to cover the gel pieces and set on ice for 30 min. After complete rehydration, excess trypsin was removed, replaced with fresh 50 mM ammonium bicarbonate, and left overnight at 37 °C. The peptides were extracted twice by the addition of 50 µl of 0.2% formic acid and 5% ACN and mixed at room temperature for 30 min. The supernatant was removed and saved. A total of 50 µl of 50% ACN, 0.2% formic acid was added to the sample, which was vortexed again at room temperature for 30 min. The supernatant was removed and combined with the supernatant from the first extraction. The combined extractions were analysed directly by liquid chromatography in combination with MS/MS using electrospray ionization. Trypsin-digested peptides were analysed by ultra-high-pressure liquid chromatography (UPLC) coupled with tandem mass spectroscopy (LC–MS/MS) using nanospray ionization. The nanospray ionization experiments were performed using a TIMS-TOF 2 pro hybrid mass spectrometer (Bruker) interfaced with nano-scale reversed-phase UPLC (EVOSEP ONE). The evosep method of 30 SPD (samples per day) was utilized using a 10 cm × 150 µm reverse-phase column packed with 1.5-µm C18-beads (PepSep, Bruker) at 58 °C. The analytical columns were connected with a fused silica ID emitter (10 µm ID; Bruker Daltonics) inside a nanoelectrospray ion source (Captive spray source; Bruker). The mobile phases comprised 0.1% formic acid as solution A and 0.1% formic acid, 99.9% ACN as solution B. The mass spectrometry settings for the TIMS-TOF Pro 2 used the PASEF method for standard proteomics. The values for mobility-dependent collision energy ramping were set to 95 eV at an inversed reduced mobility ($1/k_0$) of 1.6 V s^{-1} cm^{-2} and 23 eV at 0.73 V s^{-1} cm^{-2}. Collision energies were linearly interpolated between these two $1/k_0$ values and kept constant above or below. No merging of TIMS scans was performed. Target intensity per individual PASEF precursor was set to 20,000. The scan range was set between 0.6 and 1.6 V s^{-1} cm^{-2} with a ramp time of 166 ms. 14 PASEF MS/MS scans were triggered per cycle (2.57 s) with a maximum of seven precursors per mobilogram. Precursor ions in an m/z range between 100 and 1,700 with charge states ≥3+ and ≤8+ were selected for fragmentation. Active exclusion was enabled for 0.4 min (mass width 0.015 Th, $1/k_0$ width 0.015 V s^{-1} cm^{-2}). Protein identification and label free quantification was carried out using Peaks Studio X (Bioinformatics Solutions).

Mass spectrometry results after analysis are shown in Fig. 1b and Extended Data Fig. 1. Analysis of dataset 1 revealed the presence of the short form of γ2, and dataset 2 revealed both the short and long forms of the γ2 subunit.

Recombinant human $GABA_A$ receptor structure in complex with lamotrigine

The recombinant human α1β2γ2 $GABA_A$ receptor was expressed in a stable cell line using the Sleeping Beauty transposon system, as previously described[69]. In brief, a tri-cistronic construct encoding the three subunits was cloned into the pSBtet vector (pSBtet-GP, Addgene plasmid #60495). This was co-transfected with SB100X transposase (pCMV(CAT)T7-SB100, Addgene #34879) into HEK293S GnTI$^-$ cells (ATCC CRL-3022). These two Addgene plasmids were gifts from E. Kowarz[70] and Z. Izsvak[71], respectively. Transfected cells were selected with 1 µg ml^{-1} puromycin before being transferred to suspension culture. A total of 6.4 l of cells, at a density of 3.5 to 4 × 10^6 cells per ml were induced with 2 µg ml^{-1} doxycycline and incubated at 30 °C with shaking (130 rpm) for 48 h in 8% CO_2. To enhance expression, 3 mM sodium butyrate was added with doxycycline.

Cells were collected by centrifugation and resuspended in buffer A with 0.2 mM PMSF. After mechanical lysis, the lysate was centrifuged at 10,000*g* for 20 min. The resulting supernatant, containing cell membranes, was then centrifuged at 186,000*g* for 2 h. Membrane pellets were homogenized using a Dounce homogenizer and solubilized at 4 °C for 2 h nutating in buffer A supplemented with 1% (w/v) lauryl maltose neopentyl glycol (LMNG; Anatrace). The solubilized membranes were clarified by centrifugation at 186,000*g* for 40 min, and the supernatant was passed through a Strep-Tactin XT Superflow affinity resin (IBA-GmbH). The resin was washed with buffer A containing 1 mM LMNG and 0.01% (w/v) porcine brain polar lipids (Avanti). The protein was eluted with wash buffer supplemented with 50 mM biotin (Sigma-Aldrich).

Nanodisc reconstitution was performed using SPMSP1D1 under conditions with 0.5 mM lamotrigine. Concentrated $GABA_A$ receptors were mixed with porcine brain polar lipids (Avanti) and incubated at 4 °C for 30 min. SPMSP1D1 was then added, and the mixture was further incubated for 30 min. The final molar ratio of protein, lipids, and SPMSP1D1 was 1:100:10. To remove detergent, Bio-Beads SM2 (Bio-Rad) were added at a concentration of 100 mg ml^{-1}, and the mixture was rotated overnight at 4 °C. The next day, the Bio-Beads were removed, and the sample was collected for SEC.

Purified $GABA_A$ receptor at a concentration of 1.8 mg ml^{-1} was mixed with 0.5 mM lamotrigine and 2 mM GABA, then incubated on ice for 30 min prior to cryo-EM grid preparation. To promote random particle orientations, 0.5 mM fluorinated Fos-Choline-8 (Anatrace) was added to the protein sample just before freezing. Cryo-EM grids were prepared using a Vitrobot Mark IV (FEI). A 3 µL sample was applied to glow-discharged 200 mesh copper R 2/1 grids overlaid with 2-nm continuous carbon (Quantifoil), using 100% humidity in the chamber at 4 °C. The grids were blotted for 3.5 s and plunged into liquid ethane cooled with liquid nitrogen, then transferred to liquid nitrogen for storage.

Cryo-EM data collection was performed at the UCSD Cryo-EM Facility using the Titan Krios G4 (Thermo Fisher Scientific) operating at 300 keV and equipped with a Gatan BioContinuum energy filter. Data collection parameters are detailed in Extended Data Table 3, called dataset 3. This dataset 3 was processed using a CryoSPARC 4.4 workflow. In brief, approximately 0.7 million particles were subjected to three rounds of 2D classification to remove junk particles (Extended Data Fig. 9). A consensus map was generated by non-uniform refinement at 2.6 Å resolution. Three rounds of 3D classification focused on the TMD, followed by non-uniform refinement, yielded the final map for model building at 2.95 Å. Additionally, 3D classification and local refinement focused on the ECD improved the density of the lamotrigine-binding pocket to 2.7 Å, used for figure preparation. Both maps were uploaded to the EMDB during PDB deposition.

The human α1β2γ2 $GABA_A$ receptor bound to GABA (PDB: 6X3Z) was used as the initial model for building and refinement. Restraints for lamotrigine were generated using the Grade Web Server[72]. Manual adjustments and further refinements were performed using Coot and Phenix, as previously described. Model refinement statistics are summarized in Extended Data Table 5 (dataset 3: LTG). Structural figures were generated using UCSF ChimeraX.

Electrophysiology

Whole-cell voltage-clamp recordings were made from adherent HEK293S GnTI$^-$ cells transiently transfected with pEZT-based plasmids, as well as with GFP protein in pCDNA for cell selection. Each 10 mm well of cells in a 12-well dish was transfected with 0.1–0.4 µg plasmid mixture of each subunit in a ratio of 1 α1:1 β2 or 1 α1:1β2:10γ2 (to ensure the incorporation of γ2 subunit), using Lipofectamine 2000 reagent (Invitrogen). The transfected cells were incubated at 30 °C. After 48 h post-transfection, cells were re-plated on 35 mm dishes and allowed to settle for at least 3 h. Recordings were made 48–96 h after transfection. The bath solution contained (in mM): 140 NaCl, 2.4 KCl, 4 $MgCl_2$, 4 $CaCl_2$, 5 HEPES and 10 glucose pH 7.3. Borosilicate pipettes were pulled and polished to an initial resistance of 2–4 MΩ, filled with the pipette solution containing (in mM): 100 CsCl, 30 CsF, 10 NaCl, 10 EGTA, and 20 HEPES pH 7.3. Whole-cell currents were recorded using pClamp 11 with an Axopatch 200B amplifier, sampled at 20 kHz, and low-pass filtered at 2 kHz using a Digidata 1550B (Molecular Devices). Cells were held at −75 mV. Solution exchange was achieved using a gravity driven RSC-200 rapid solution changer (Bio-Logic). Whole-cell currents were analysed with Clampfit 11 software (Molecular Devices). GABA and ligand (lamotrigine, levetiracetam, lacosamide, and zonisamide, Sigma-Aldrich) solutions were prepared in bath solution from concentrated stocks: 1 M GABA in water, and 300 mM lamotrigine, 500 mM Levetiracetam, 300 mM lacosamide and 300 mM zonisamide in DMSO. For the statistics in Fig. 3 (bar graph), results are presented as normalized peak currents. Rundown was consistently observed in α1β2 recordings; repeated measurements of the response to GABA application were made until stable peak currents were observed, then the drug applications were tested. We observed that only half of the cells expressing the α1β2 receptors responded to levetiracetam and lamotrigine; we report in Fig. 3e the currents from responsive cells. Replicate numbers from independent cells are labelled in each bar. Statistical analysis was performed using GraphPad Prism 10.2.0 software (GraphPad Software). Data are expressed as mean ± s.d. Two-tailed Welch's *t*-test was used. A *P* value of ≤0.05 was considered statistically significant (***$P \leq 0.001$; **$P \leq 0.01$; $0.01 \leq$ *$P \leq 0.05$).

Reporting summary

Further information on research design is available in the Nature Portfolio Reporting Summary linked to this article.

Data availability

All atomic models and cryo-EM maps have been deposited in the Protein Data Bank (PDB) and Electron Microscopy Data Bank (EMDB): β2–α1–β2–α1–γ2 (PDB 9CRS, EMD-45878), β2–α1–γ2–β2–α2 (PDB 9CRV, EMD-45884), β3–α1–β2–α2–γ2 (PDB 9CSB, EMD-45890), β2–α1–β2–α2–γ2 (PDB 9CT0, EMD-45894), β2–α1–β3–α2–γ2 (PDB 9CTJ, EMD-45908), β2–α1–β2–α3–γ2 (PDB 9CTP, EMD-45914), β2–α1–γ2–β1–α2 (PDB 9CTV, EMD-45920), β2–α1–β3–α1–γ2 (PDB 9CXA, EMD-45983), β3–α1–γ2–β2–α2 (PDB 9CXC, EMD-45985), β3–α1–γ2–β3–α2 (PDB 9CX7, EMD-45980), β2–α1–β1–α2–γ2 (PDB 9CXB, EMD-45984), β2–α1–β1–β1–γ2 (PDB 9CXD, EMD-45986), lamotrigine-bound β2–α1–β2–α1–γ2 (PDB 9DRX, EMD-47132). Raw electrophysiology and mass spectrometry data are included as Source data with this paper.

62. Punjani, A., Rubinstein, J. L., Fleet, D. J. & Brubaker, M. A. cryoSPARC: algorithms for rapid unsupervised cryo-EM structure determination. *Nat. Methods* **14**, 290–296 (2017).
63. Pettersen, E. F. et al. UCSF ChimeraX: structure visualization for researchers, educators, and developers. *Protein Sci.* **30**, 70–82 (2021).
64. Emsley, P., Lohkamp, B., Scott, W. G. & Cowtan, K. Features and development of Coot. *Acta Crystallogr. D* **66**, 486–501 (2010).
65. Afonine, P. V. et al. Real-space refinement in PHENIX for cryo-EM and crystallography. *Acta Crystallogr. D* **74**, 531–544 (2018).
66. Williams, C. J. et al. MolProbity: more and better reference data for improved all-atom structure validation. *Protein Sci.* **27**, 293–315 (2018).
67. Smart, O. S., Neduvelil, J. G., Wang, X., Wallace, B. A. & Sansom, M. S. HOLE: a program for the analysis of the pore dimensions of ion channel structural models. *J. Mol. Graph.* **14**, 354–360, 376 (1996).
68. Shevchenko, A., Wilm, M., Vorm, O. & Mann, M. Mass spectrometric sequencing of proteins silver-stained polyacrylamide gels. *Anal. Chem.* **68**, 850–858 (1996).
69. Chojnacka, W., Teng, J., Kim, J. J., Jensen, A. A. & Hibbs, R. E. Structural insights into $GABA_A$ receptor potentiation by Quaalude. *Nat. Commun.* **15**, 5244 (2024).
70. Kowarz, E., Loscher, D. & Marschalek, R. Optimized Sleeping Beauty transposons rapidly generate stable transgenic cell lines. *Biotechnol. J.* **10**, 647–653 (2015).
71. Mates, L. et al. Molecular evolution of a novel hyperactive Sleeping Beauty transposase enables robust stable gene transfer in vertebrates. *Nat. Genet.* **41**, 753–761 (2009).
72. Smart, O.S. et al. Grade2 v.1.6.0. (Global Phasing Ltd., 2021).
73. Laverty, D. et al. Cryo-EM structure of the human α1β3γ2 $GABA_A$ receptor in a lipid bilayer. *Nature* **565**, 516–520 (2019).

Acknowledgements We are grateful to the patients and their families for providing the brain tissue and access to enable research. The authors thank H. Jiang, A. Marinas, S. Burke, H. Li and W. Chojnacka for discussions and manuscript review; L. Baxter for assistance with figures; the UC San Diego Cryo-EM Facility for their scientific and technical support; M. Matyszewski for discussions and assistance with data collection and processing; A. Lemoff and M. Ghassemian for their support with mass spectrometry; G. Konopka and M. Harper for facilitating surgical tissue preparation and storage; and S. Tomita for discussions and preliminary experiments with synaptic interacting proteins. This work was supported by grants from the American Heart Association (24POST1195454 to J.Z.) and from the NIH (NS132443 to H.M., NS126143 to B.L. and DA047325 to R.E.H.).

Author contributions J.Z. performed the biochemistry, cryo-EM sample preparation, data processing, model building, refinement, structural analysis and drafted and revised the manuscript. C.M.N. performed model building and manuscript revision. J.T. performed the electrophysiology experiments. H.M. collected and prepared tissue. B.L. performed surgeries. R.E.H. provided oversight for the project and drafted and revised the manuscript with all authors.

Competing interests The authors declare no competing interests.

Additional information

Supplementary information The online version contains supplementary material available at https://doi.org/10.1038/s41586-024-08454-1.

Correspondence and requests for materials should be addressed to Ryan E. Hibbs.

Peer review information *Nature* thanks Pierre-Jean Corringer, Bryndis Birnir and the other, anonymous, reviewer(s) for their contribution to the peer review of this work. Peer reviewer reports are available.

Reprints and permissions information is available at http://www.nature.com/reprints.

a

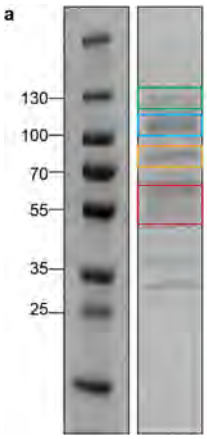

b

Protein	Coverage(%)	Peptides	Abundance
Human α1	77	41	3.61×10^{9}
Human α2	67	27	9.77×10^{7}
Human α3	60	26	7.21×10^{7}
Human α4	45	20	2.71×10^{7}
Human α5	52	20	3.28×10^{7}
Human α6	14	4	1.75×10^{4}
Human β1	47	25	1.86×10^{8}
Human β2	45	28	1.56×10^{9}
Human β3	41	22	5.26×10^{8}
Human γ1	39	14	2.18×10^{7}
Human γ2	46	24	6.25×10^{8}
Human γ3	7	2	2.48×10^{5}
Human δ	49	17	3.22×10^{7}

c

Protein	Coverage(%)	Peptides	Abundance
Neuroligin2	60	41	1.11×10^{9}
Neuroligin4X	41	25	6.84×10^{7}
Neuroligin4Y	41	24	2.67×10^{8}
Neuroligin3	50	25	8.20×10^{7}
Neuroligin1	41	23	2.26×10^{7}
SV2B	60	40	5.71×10^{9}
SV2A	40	20	4.27×10^{7}
SYT1	71	50	8.59×10^{9}
SYT2	64	23	4.29×10^{7}
SYT5	10	5	1.71×10^{5}
SYT12	55	17	6.51×10^{8}

Extended Data Fig. 1 | Characterization of native human α1-containing $GABA_A$ receptors and associated proteins from brain tissue. a, Sample analysis focus on the $GABA_AR$ and non-$GABA_AR$ bands. **b**, Same analysis conducted as in Fig. 1b. **c**, The top three unknown bands in the SDS-PAGE gel were individually excised for mass spectrometry analysis. Detailed results regarding associated proteins and their related homologues are provided in the table. The table groups are color-coded to match the boxes in **a**. Results shown in this representative gel were similarly obtained from n = 4 gels from independent purifications. Molecular weights of standards are given on the left of the gel in kD. Uncropped SDS-PAGE gel is provided in Supplementary Fig. 1.

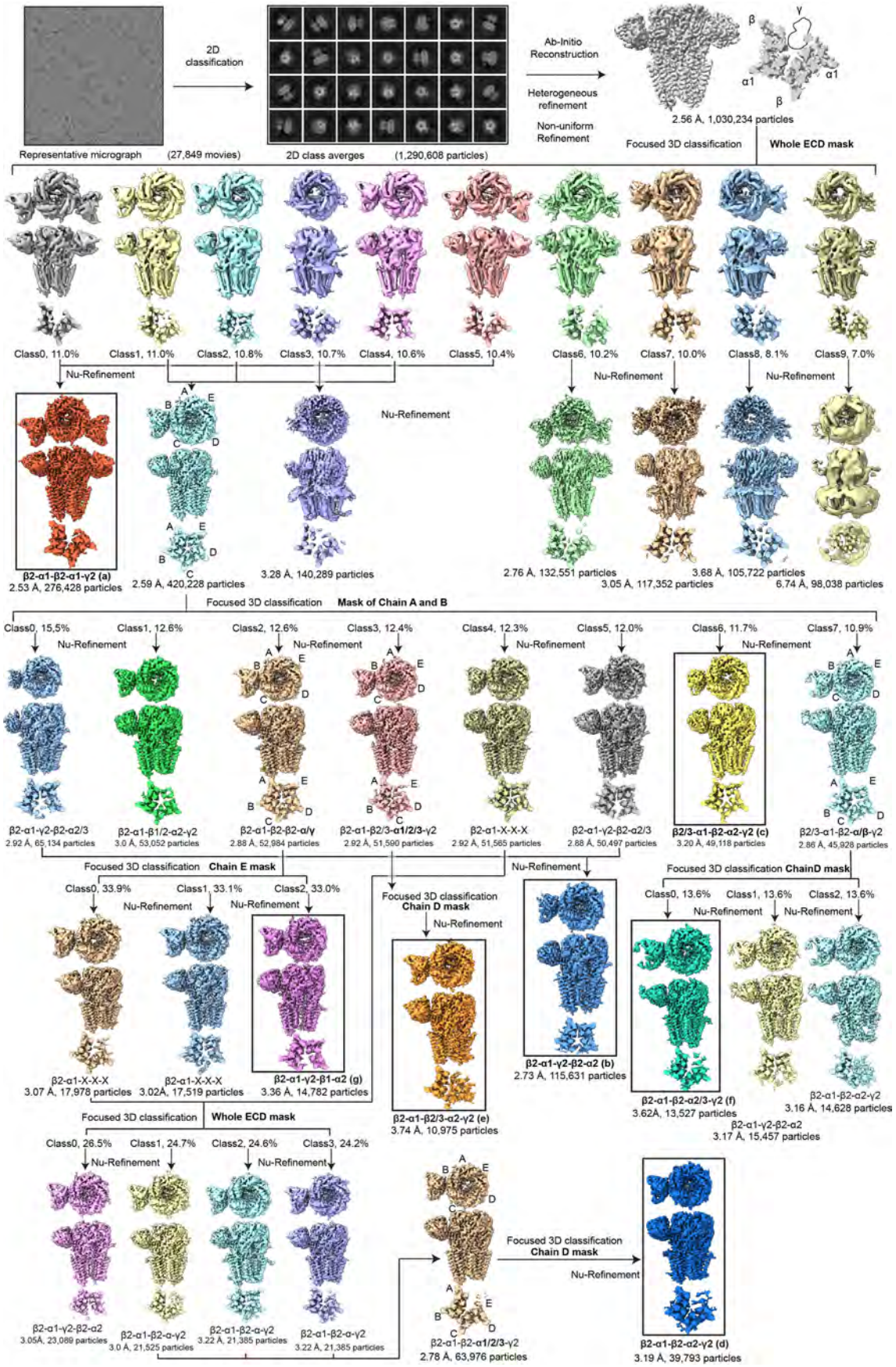

Extended Data Fig. 2 | See next page for caption.

Extended Data Fig. 2 | Cryo-EM data processing of Dataset 1 from tissue from 45 patients. ~28k dose-fractionated micrographs were collected from multiple grids stemming from one purification using anti-α1 Fab (1F4) as the affinity reagent. All data processing was performed in CryoSPARC v4.4. Particles were picked and subjected to multiple rounds of 2D classification; final results are shown, with ~1.3 M particles selected from this step. Ab initio reconstruction was performed with 3 classes, which were used as inputs for heterogeneous refinement of the whole particle set. A single particle set emerged from heterogeneous refinement including ~1.0 M particles, which was subjected to non-uniform (NU) refinement. This map and particle set served as the starting point for all 3D classification. The primary 3D classification used a focused mask around the whole ECD and was set up with 10 classes (Class0 - Class9). The ECD mask was chosen due to the highest resolution features being mainly found in the ECD, and thus this region should allow more robust separation of compositional heterogeneity. Class0 and Class5 contained two strong Fab densities, so were combined and refined to a single subunit arrangement easily definable during model building as β2-α1-β2-α1-γ2. This map and subunit arrangement are indicated as a final, high confidence endpoint in this data processing by listing the subunit order in bold font. The FSC-based map resolution estimate and particle number are given below all maps. Classes 1, 2, and 4 were pooled due to the presence of one strong Fab, refined, and yielded a ~2.6 Å resolution map. Heterogeneity in TMD signal in the input classes (1, 2, 4) motivated us to conduct a secondary 3D classification on this ~420k particle set (8 classes). Briefly, however, from the primary 3D classification, Class3 and Class6-Class9 were excluded from further analysis due to anisotropic resolution features suggestive of preferred orientation, or low resolution overall (Class3 and 9). Secondary classification of 1-Fab containing particles using focus map on Chains A-B ECD. This region was selected for masking after testing a large panel of masks (single subunits, pairs, adjacent triplets). All 3D classes were subjected to Nu refinement, then atomic model building was done to begin assigning subunits to map positions (Supplementary Figs. 1–11). Class0 and Class5 exhibited features of a common assembly, so were pooled and refined, to a final subunit arrangement of β2-α1-γ2-β2-α2. All processing is summarized in this flow chart for the dataset with the above explanations serving as representative decision-making approaches. Each composition has been also labeled as (a-g), corresponding to the labels in Fig. 2 and Extended Data Fig. 6. In some cases, a single position in a map was clearly a mixture of two subunits, for example α2/α3. In other cases, we designate the heterogeneity as a "mixture," which instead means that one or more positions are not yet at that step clearly an α vs. β vs. γ. While we cannot rule out the possibility of contamination in a "final" particle set, arising from a minor fraction of incorrect particles, we can conclude with confidence that for each of the "final" maps, the model built represents the clearly dominant species in that particle set.

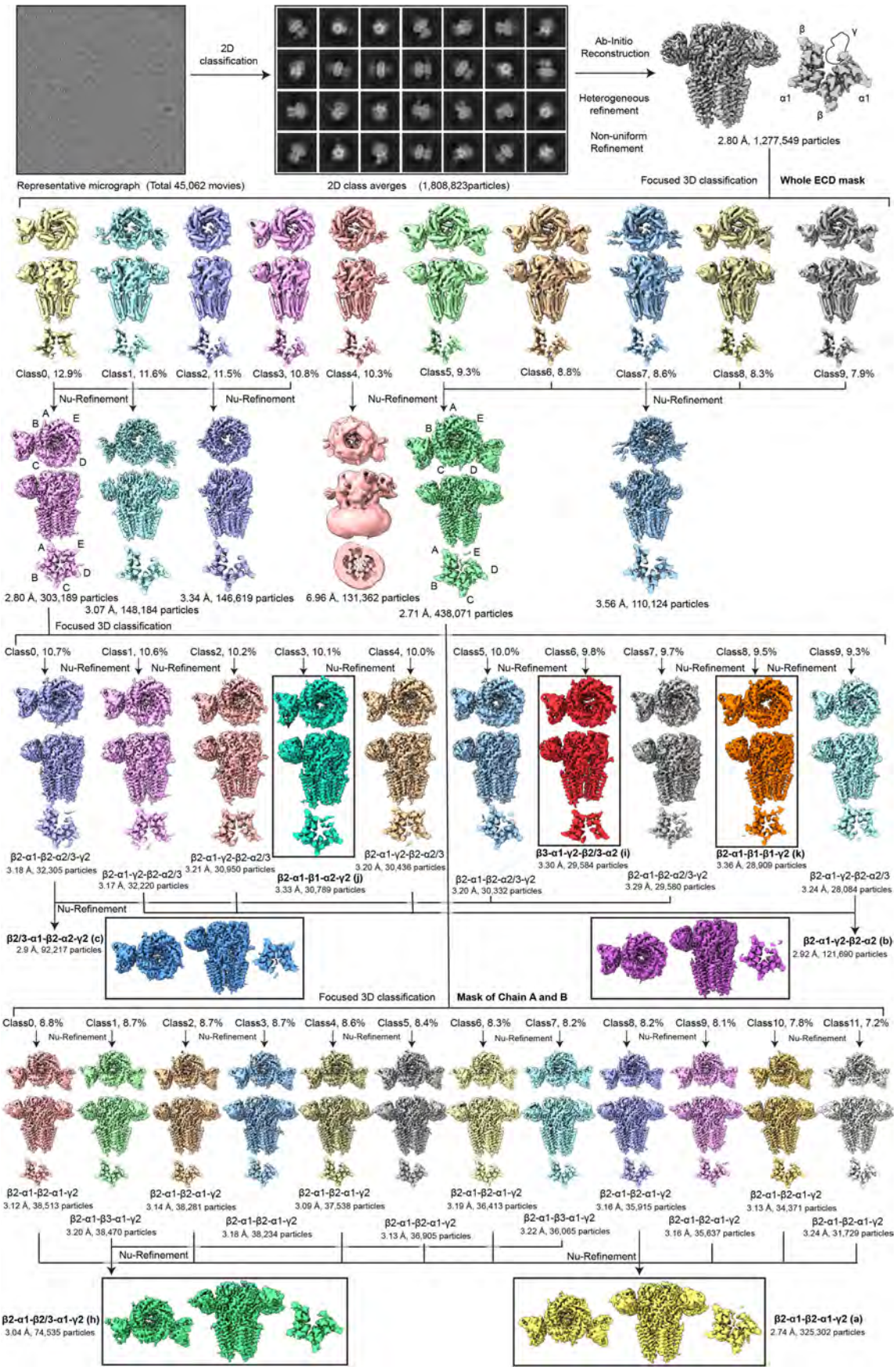

Extended Data Fig. 3 | See next page for caption.

Extended Data Fig. 3 | Cryo-EM data processing of Dataset 2 from tissue from 36 patients. Approximately 45k dose-fractionated micrographs were collected, resulting in 1.8 million particles after several rounds of 2D classification. The workflow was conducted according to the procedures outlined in Extended Data Fig. 2. All models were constructed for the reconstructions highlighted in the back boxes. Each composition is also labeled as (a-c) and (h-k), corresponding to the labels in Fig. 2 and Extended Data Fig. 6.

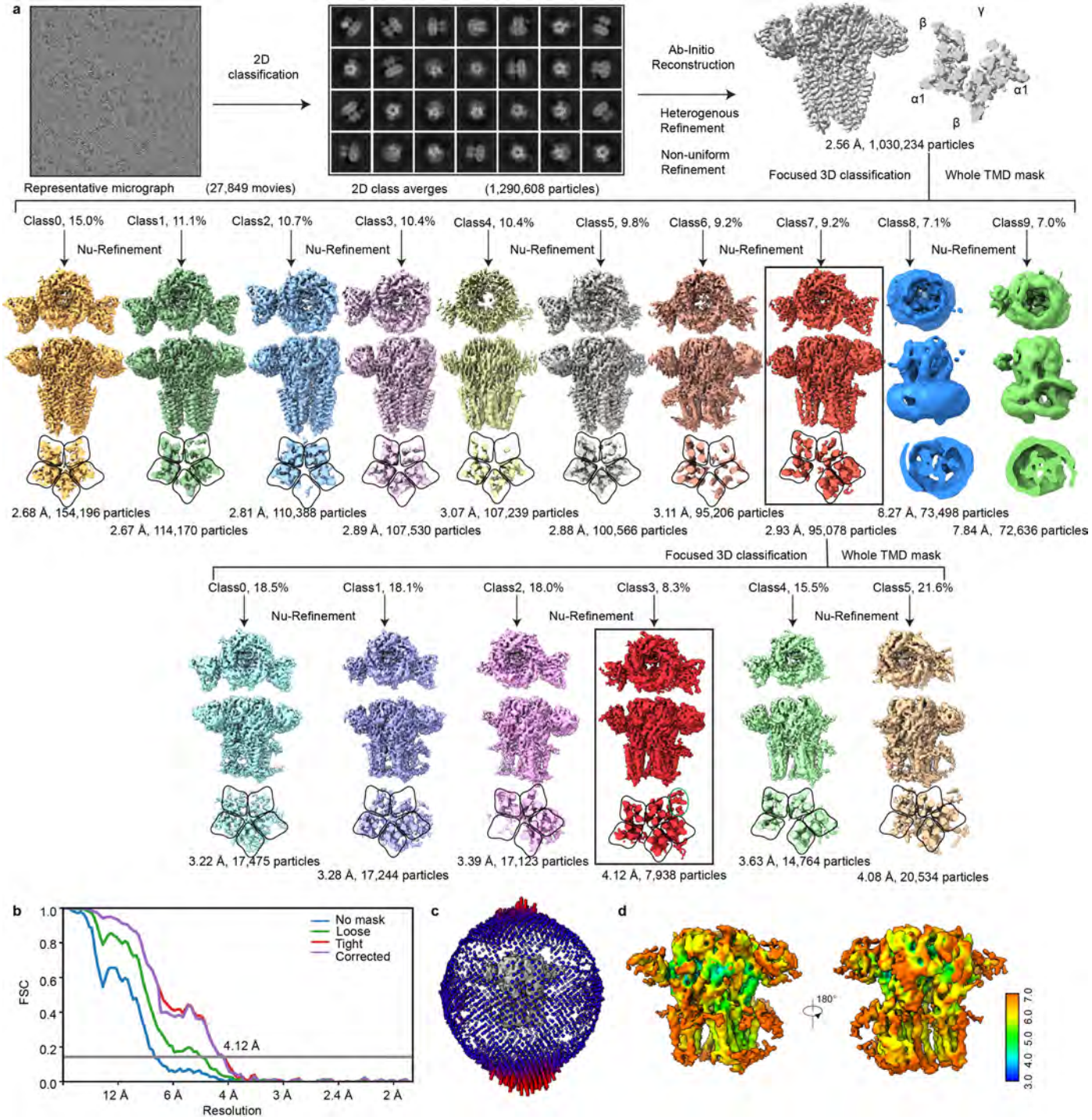

Extended Data Fig. 4 | Cryo-EM analysis of the native α1-containing $GABA_A$ receptors in complex with interacting partner density. a, Single-particle cryo-EM image processing workflow, focusing on the transmembrane domain (TMD). Refer to the Methods section for further elaboration on the workflow. Fourier shell correlation (FSC) curves with gray line indicating FSC = 0.143 (**b**), angular distribution plot (**c**) and local-resolution maps (**d**) for the final 3D reconstruction.

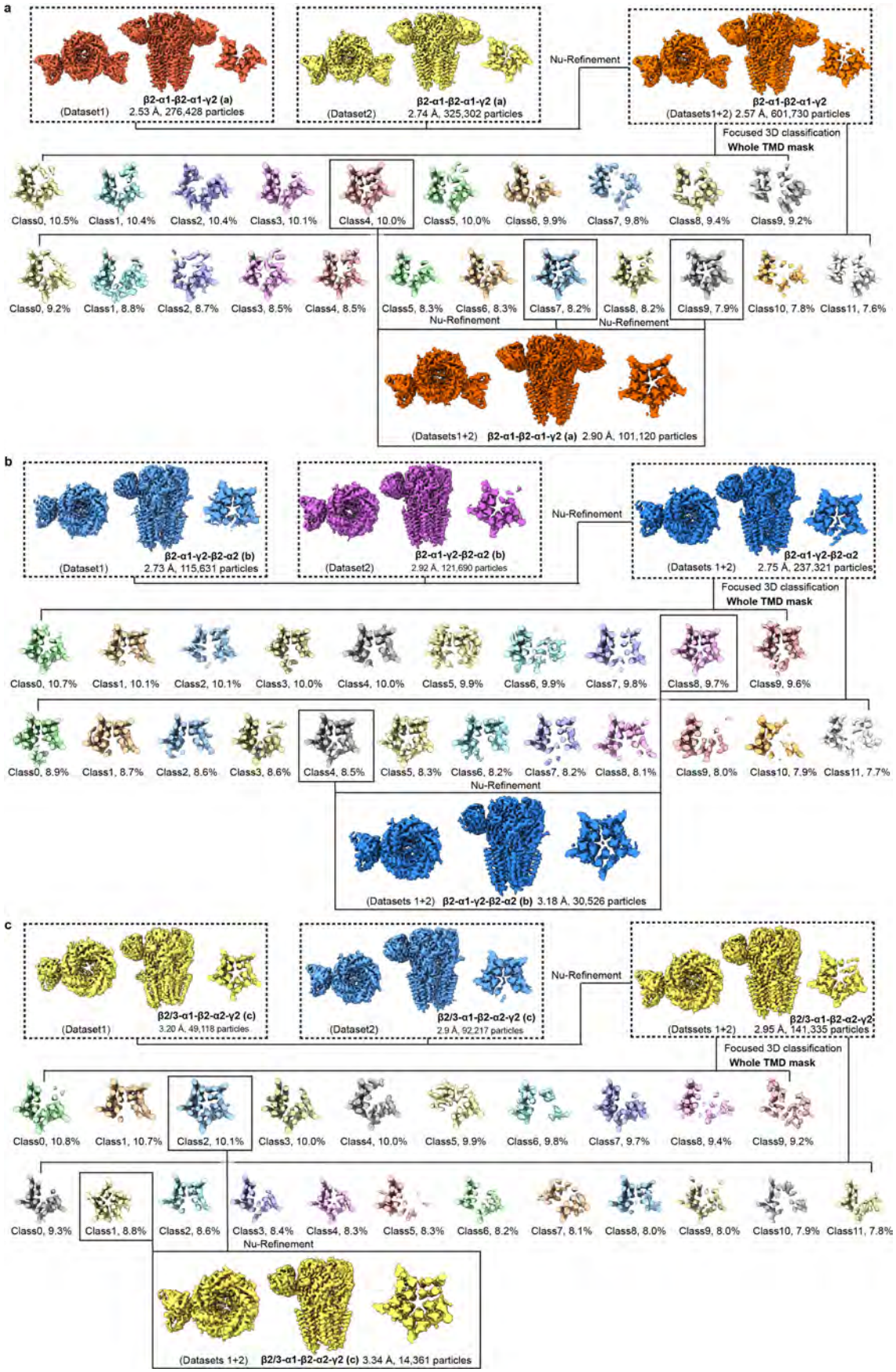

Extended Data Fig. 5 | See next page for caption.

Extended Data Fig. 5 | Focused classification for γ2-TMD map reconstruction in the three subunit compositions abundant in both datasets. All cryo-EM data processing steps were performed using CryoSPARC v4.4. Further NU refinement combined particles from both datasets. Focused 3D classifications on the entire TMD region were conducted, and the class with a strong γ2 subunit signal was selected for the final reconstruction. All models were constructed for the reconstructions highlighted in the outlined black boxes. The determination of the γ2 subunit in the compositions β2-α1-β2-α1-γ2, β2-α1-γ2-β2-α2, and β2/3-α1-β2-α1-γ2 is displayed in panels **a**, **b**, and **c**, respectively. Each final composition is also labeled as (a-c), corresponding to the labels in Fig. 2 and Extended Data Fig. 6.

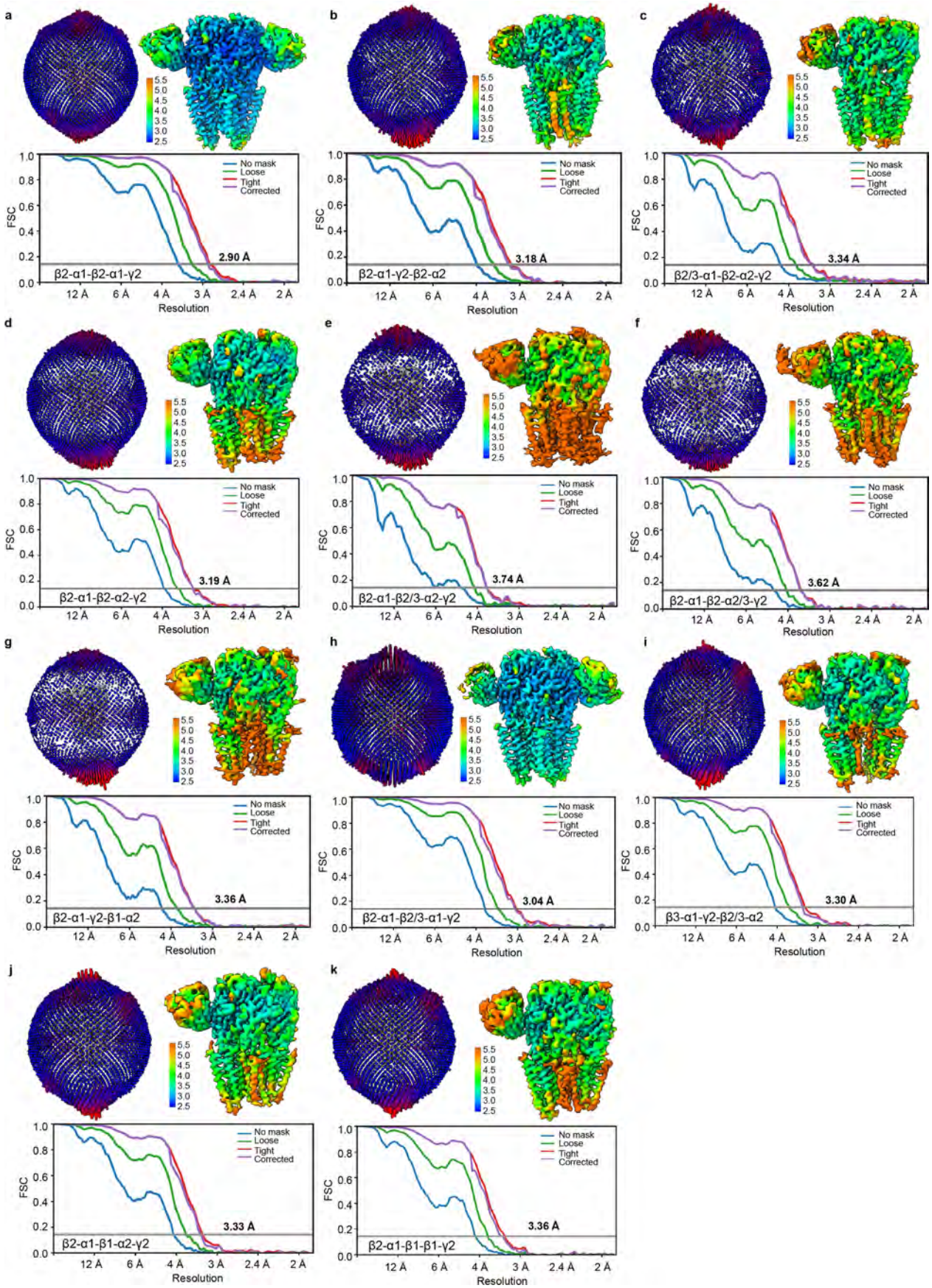

Extended Data Fig. 6 | See next page for caption.

Extended Data Fig. 6 | Characteristics of cryo-EM reconstructions. The angular distribution plots of particles used for the final cryo-EM reconstructions are shown in the top left. The cryo-EM maps, colored according to local resolution estimation in CryoSPARC v4.4, are displayed in the top right (color scale in Å). FSC curves were calculated between half-maps, with the overall resolution estimated using the FSC = 0.143 criterion (below). The detailed compositions of the eleven cryo-EM maps are labeled in the tables of FSC curves.

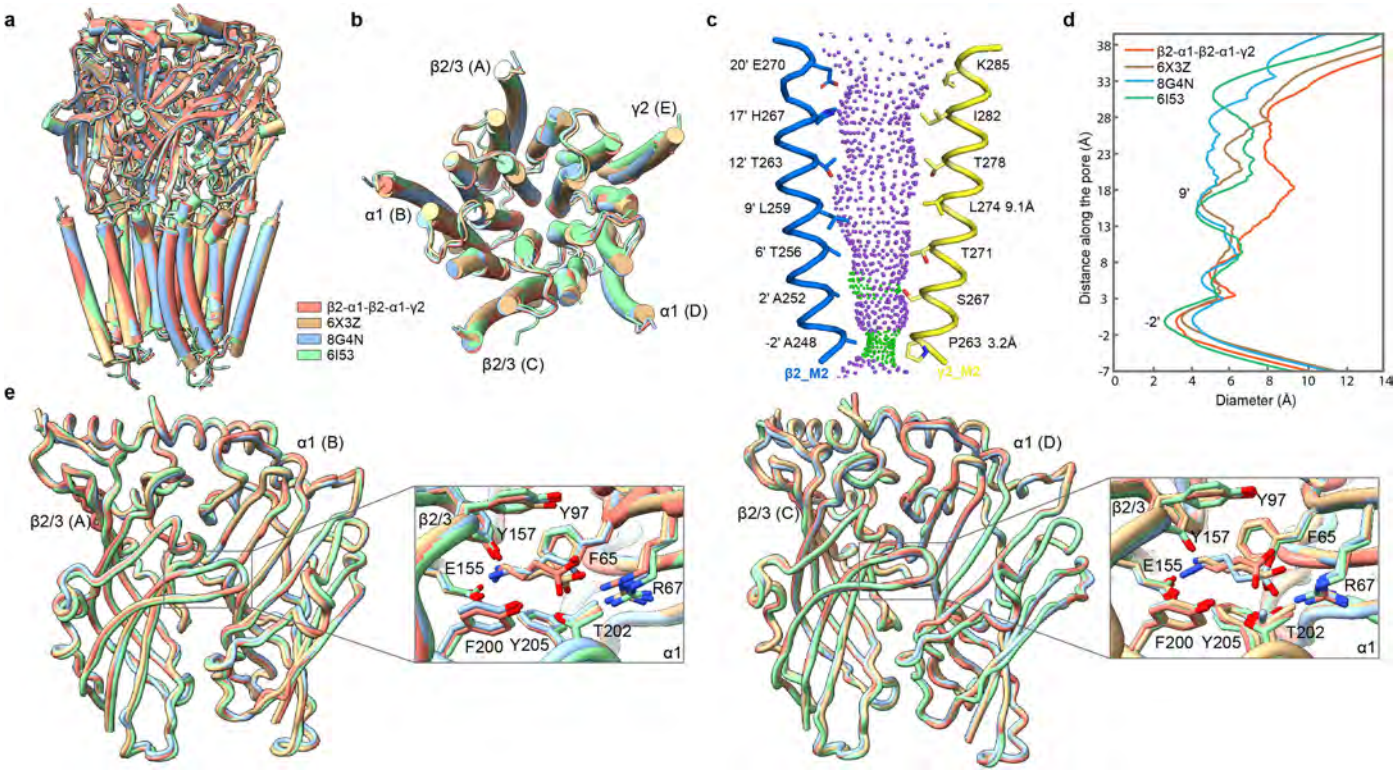

Extended Data Fig. 7 | Comparative analysis of the most abundant native $GABA_A$ receptor with previously reported structures. a, Structural comparison of the β2-α1-β2-α1-γ2 (light coral) with 6X3Z[37] (burly wood), 6I53[73] (light green), and 8G4N[8] (sky blue) demonstrates high overall similarity. **b**, Detailed comparison of the transmembrane domain regions, with colors consistent with panel **a**. Each subunit is labeled accordingly. **c**, Pore conformation of the β2-α1-β2-α1-γ2 receptor, highlighting the opposing β2 and γ2 M2 α-helices as ribbons, with the pore-lining side chains shown as sticks. Purple and green spheres illustrate the pore shape. Distances shown within the pore represent diameters at the desensitization gate (−2′) and resting gate (9′) positions. **d**, Comparative pore diameter versus distance plot for the structures depicted in panel **a**, aligned at y = 0 at the level of the -2′ desensitization gate. **e**, Superposition of structures based on the extracellular domains of adjacent β and α subunits, as shown in panel **a**.

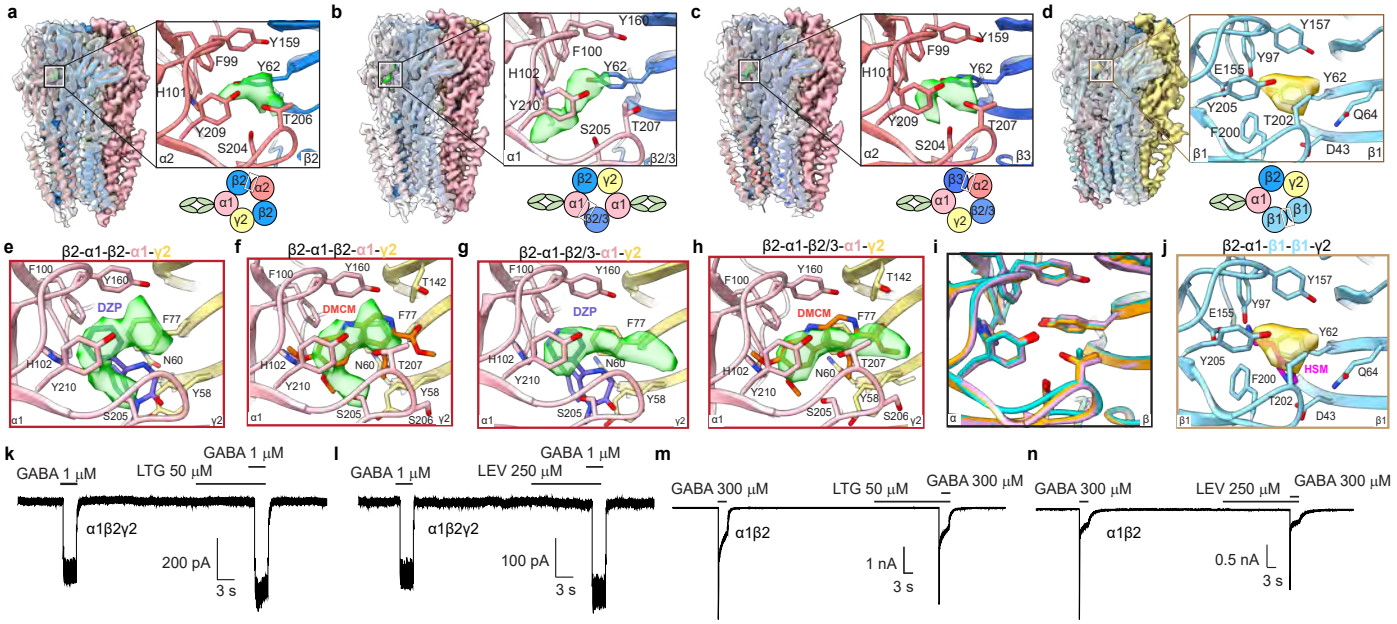

Extended Data Fig. 8 | Densities in native α1-containing $GABA_A$ receptors, ligand docking and electrophysiological recordings. Cryo-EM densities were observed at the interfaces formed by the ECDs of the α and β subunits in the composition of β2-α1-γ2-β2-α2 (**a**), β2-α1-β2/3-α1-γ2 (**b**) and β3-α1-γ2-β2/3-α2 (**c**). Additionally, density was observed at the interfaces formed by the ECDs of the β1 and β1 subunits in the composition of β2-α1-β1-β1-γ2 (**d**). Ligands of diazepam (DZP) and DMCM aligned with the composition of β2-α1-β2-α1-γ2 (**e**, **f**) and β2-α1-β2/3-α1-γ2 (**g**, **h**) at the interface of α1 and γ2 subunits. DZP pose is from PDB: 6X3X[37] and DMCM from PDB: 8DD3[39]. **i**, Superposition of surrounding residues from the compositions of β2-α1-γ2-β2-α2, β2-α1-β2/3-α1-γ2 and β3-α1-γ2-β2/3-α2 at interfaces of α and β subunits. **j**, The alignment of histamine (HSM) with the composition of β2-α1-β1-β1-γ2 at the interface of β1 and β1 subunits; histamine binding pose from Sente et al.[5]. **k-l**, Representative responses are shown for application of GABA, followed by GABA plus LTG with α1β2γ2 and α1β2, and same for LEV (**m-n**).

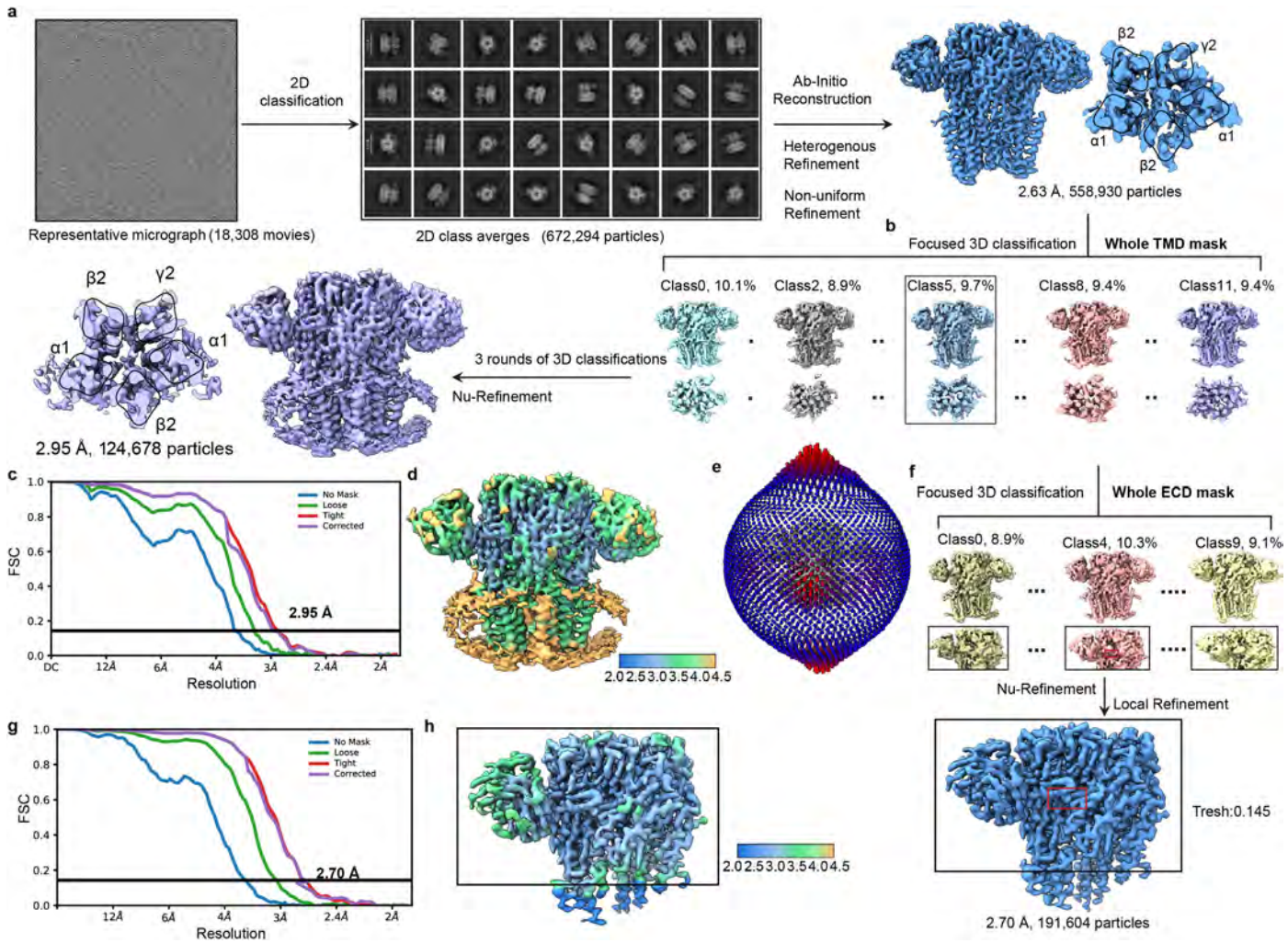

Extended Data Fig. 9 | Cryo-EM analysis of recombinant $GABA_A$ receptor in complex with lamotrigine. a, Single-particle cryo-EM image processing workflow, with several rounds of focused 3D classification on the transmembrane domain (TMD), as shown in **b**. **c**, Fourier shell correlation (FSC) curves, with the gray line indicating FSC = 0.143. **d**, Local-resolution map and **e**, angular distribution plot for the final 3D reconstruction. To enhance lamotrigine density, focused 3D classification and local refinement were applied to the extracellular domain (ECD), as shown in **f**. **g**, FSC curves, with the gray line indicating FSC = 0.143, and **h**, local-resolution maps for the final 3D reconstruction. In **f** and **h**, black box boundaries approximate mask used in focused refinement and local resolution estimate; local resolution for regions outside of the mask (e.g., TMD helices) are not meaningful.

Extended Data Table 1 | Characteristics of 45 Epilepsy Patients

Sample	Age	Sex	Region	AEDs at time of surgery	Epilepsy duration (y)
25	35	M	Temporal	Phenytoin, Zonisamide	25
26	56	M	Temporal	Lacosamide, Lamotrigine	19
27	33	F	Temporal	Carbamazepine,Lamotrigine, Levetiracetam	26
28	43	F	Temporal	Lamotrigine, Topiramate	17
29	46	M	Temporal	Zonisamide, Lacosamide, Gabapentin,Valproate	9
30	74	M	Temporal	Brivaracetam, Zonisamide	3
35	22	M	Temporal	Brivaracetam, Lacosamide	9
37	64	M	Temporal	Lacosamide, Levetiracetam	8
39	22	M	Temporal	Lacosamide, Topiramate	3
40	45	M	Temporal	Levetiracetam, Oxcarbazepine	41
42	51	F	Temporal	Zonisamide, Lacosamide, Gabapentin, Valproate	50
43	29	M	Temporal	Clobazam, Lacosamide, Levetiracetam	28
48	50	F	Temporal	Phenytoin, Lacosamide,Gabapentin	4
52	24	F	Temporal	Levetiracetam, Oxcarbazepine	1
53	51	M	Temporal	Phenytoin, Gabapentin	43
57	59	F	Temporal	Carbamazepine, Clonazepam	36
58	68	F	Temporal	Lacosamide	23
59	38	F	Temporal	Eslicarbazepine	31
63	26	M	Temporal	Brivaracetam, Eslicarbazepine	1.5
65	35	F	Temporal	Unknown	2
66	54	F	Temporal	Lacosamide, Clobazam, Brivaracetam	22
70	29	M	Temporal	Lacosamide, Zonisamide	10
72	33	M	Temporal	Lamotrigine	4
74	36	M	Temporal	Carbamazepine, Levetiracetam	18
75	36	F	Temporal	Lamotrigine, Levetiracetam, Oxcarbazepine	31
76	24	M	Temporal	Lamotrigine, Zonisamide	16
77	23	M	Temporal	Brivaracetam, Lacosamide	10
78	54	F	Temporal	Eslicarbazepine, Lamotrigine	5
82	37	F	Temporal	Lamotrigine	5
83	23	F	Temporal	Lacosamide, Levetiracetam	5
84	44	F	Temporal	Levetiracetam, Lamotrigine, Lacosamide	41
85	19	M	Temporal	Lacosamide, Lamotrigine	11
87	35	F	Temporal	Brivaracetam, Lamotrigine	25
88	34	F	Temporal	Eslicarbazepine, Cenobamate	4
89	57	F	Temporal	Lacosamide	11
90	46	M	Temporal	Brivaracetam, Lamotrigine	12
91	51	M	Frontal	Lacosamide, Clonazepam	17
92	55	F	Temporal	Lacosamide, Topiramate	15
94	43	M	Frontal	Zonisamide	4
95	21	F	Temporal	Oxcarbazepine, Phenobarbital, Clonazepam, Lacosamide, Levetiracetam,Pregabalin	7
96	67	F	Frontal	Zonisamide	25
97	31	M	Frontal	Lamotrigine, Levetiracetam	15
98	44	M	Temporal	Carbamazepine, Lamotrigine, Levetiracetam	5
99	58	F	Temporal	Zonisamide, Gabapentin	5
100	50	M	Temporal	Lacosamide, Oxcarbazepine	20

Table summarizing information on 45-patient samples, including age, sex, brain region (temporal or frontal lobe), antiepileptic drugs administered to patients, and the duration of epilepsy (in years).

Extended Data Table 2 | Characteristics of 36 Epilepsy Patients

Sample	Age	Sex	Region	Antiepileptic drugs at time of surgery	Epilepsy duration (y)
101	31	M	Temporal	Valproate, Lamotrigine	7
102	26	F	Temporal	Lacosamide	10
103	44	F	Frontal	Phenytoin	22
106	31	M	Temporal	Lacosamide, Topiramate	2
107	57	M	Temporal	Clobazam, Carbamazepine, Levetiracetam	27
108	40	M	Temporal	Oxcarbazepine, Zonisamide	2
109	40	M	Temporal	Carbamazepine, Lacosamide	40
110	47	F	Temporal	Carbamazepine, Lamotrigine	28
130	48	M	Temporal	Topiramate, Carbamazepine, Lamotrigine	45
131	61	M	Temporal	Levetiracetam	53
132	59	M	Temporal	Lacosamide, Oxcarbazepine	5
133	59	M	Temporal	Eslicarbazepine	20
134	25	M	Temporal	Valproate, Levetiracetam	1
135	55	M	Temporal	Lamotrigine	13
138	55	M	Temporal	Lacosamide, Lamotrigine	51
141	36	M	Temporal	Oxcarbazepine	2
142	64	M	Temporal	Lacosamide, Levetiracetam	62
143	45	M	Temporal	Zonisamide, Oxcarbazepine	32
144	28	M	Temporal	Brivaracetam, Lamotrigine	15
145	37	F	Frontal	Zonisamide, Lacosamide, Lamotrigine, Levetiracetam	3
146	43	M	Frontal	Zonisamide, Lacosamide, Levetiracetam	5
147	41	F	Temporal	Fosphenytoin, Levetiracetam	3
148	26	M	Temporal	Lacosamide, Oxcarbazepine	7
149	44	M	Temporal	Lamotrigine, Levetiracetam	18
150	33	M	Temporal	Zonisamide, Levetiracetam	18
153	38	F	Temporal	Lamotrigine, Levetiracetam	20
154	58	M	Temporal	Zonisamide, Lacosamide	7
155	41	F	Temporal	Zonisamide, Levetiracetam, Lamotrigine	38
156	42	F	Temporal	Lacosamide, Lamotrigine	37
158	49	M	Frontal	Brivaracetam, Lacosamide, Cenobamate	35
159	41	F	Temporal	Levetiracetam	21
162	23	M	Temporal	Cenobamate, Lamotrigine, Levetiracetam	4
163	31	F	Temporal	Fosphenytoin, Lamotrigine	12
165	23	M	Temporal	Valproate, Levetiracetam, Lacosamide, Fosphenytoin	20
166	39	M	Temporal	Lacosamide, Levetiracetam	36
167	38	M	Frontal	Felbamate, Fosphenytoin, Lacosamide, Lamotrigine, Levetiracetam	33

Table summarizing information on 36-patient samples, including age, sex, brain region (temporal or frontal lobe), antiepileptic drugs administered to patients, and the duration of epilepsy (in years).

Extended Data Table 3 | Cryo-EM data collection parameters

	Dataset1 Native $GABA_AR$ (+GABA)	Dataset2 Native $GABA_AR$ (+GABA)	Dataset3 $GABA_AR$ (+GABA and LTG)
Data collection and processing			
Microscope	UCSD Krios G4	UCSD Krios G4	UCSD Krios G4
Electron Gun	FEG	FEG	FEG
Detector	Falcon4	Falcon4	Falcon4
Magnification	130K	130K	130K
Voltage (kV)	300	300	300
Electron exposure ($e^{-}/Å^2$)	50	50	50
Defocus range (μm)	1.0 - 2.2	1.0 - 2.2	1.0 - 2.2
Pixel size (Å)	0.935	0.935	0.935
Symmetry imposed	C1	C1	C1
Number of collected movies	27,849	45,062	18,308
Initial particle images (no.)	1,290,608	1,808,823	789,923

Table summarizing cryo-EM data collection and processing statistics for the 3 datasets in this study.

Extended Data Table 4 | Refinement and validation statistics

Dataset	Dataset1+2	Dataset1+2	Dataset1+2	Dataset1	Dataset1	Dataset1	Dataset1
Map	β2-α1-β2-α1-γ2	β2-α1-γ2-β2-α2	β2/3-α1-β2-α2-γ2	β2 -α1 -β2 -α2 -γ2	β2 -α1 -β2/3 -α2 -γ2	β2 -α1 -β2 -α2/3 -γ2	β2-α1-γ2-β1-α2
Model	β2-α1-β2-α1-γ2	β2-α1-γ2-β2-α2	β3-α1-β2-α2-γ2	β2 -α1 -β2 -α2 -γ2	β2 -α1 -β3 -α2 -γ2	β2 -α1 -β2 -α3 -γ2	β2-α1-γ2-β1-α2
EMDB ID	EMD-45878	EMD-45884	EMD-45890	EMD-45894	EMD-45908	EMD-45914	EMD-45920
PDB ID	9CRS	9CRV	9CSB	9CT0	9CTJ	9CTP	9CTV
Initial model used (PDB code)	6X3T/6I53	6X3T/6I53	6X3T/6I53	6X3T/6I53	6X3T/6I53	6X3T/6I53	6X3T/6I53
Final particle images (no.)	101,120	30,526	14,361	39,793	10,975	13,527	14,782
Map resolution (Å) FSC threshold=0.143	2.90	3.18	3.34	3.19	3.74	3.62	3.36
Map sharpening *B* factor (Å^2)	87.1	70.5	57.0	74.3	54.1	53.8	53.8
Model composition							
Non-hydrogen atoms	17, 623	15, 727	155,25	14,736	14, 479	14, 609	14, 578
Protein residues	2122	1886	1873	1761	1755	1751	1751
Glycans	22	21	16	19	19	17	19
Ligands	4	4	1	4	0	2	2
Lipids	2	1	2	2	0	2	1
***B* factors (Å^2)**							
Protein	66.45	79.80	103.26	95.86	129.00	113.03	104.00
Ligands	79.93	102.99	166.91	145.7	103.32	131.68	131.91
R.m.s. deviations							
Bond lengths (Å)	0.006	0.006	0.007	0.007	0.007	0.007	0.006
Bond angles (°)	0.972	0.877	1.000	1.080	1.087	1.075	0.873
Validation							
MolProbity score	1.56	1.62	1.89	1.97	2.09	1.88	1.54
Clashscore	5.10	5.94	7.42	7.65	8.71	8.51	6.07
Poor rotamers (%)	0.90	0.65	1.37	1.58	1.97	1.14	0.57
Ramachandran plot							
Favored (%)	95.85	95.80	94.54	94.02	94.00	94.45	96.76
Allowed (%)	4.15	4.20	5.46	5.98	6.00	5.55	3.24
Disallowed (%)	0	0	0	0	0	0	0

Table summarizing cryo-EM data refinement and validation statistics for 7 of the native receptor maps and models generated in this study.

Extended Data Table 5 | Refinement and validation statistics

Dataset	Dataset2	Dataset2	Dataset2	Dataset2	Dataset2	Dataset3: LTG
Map	β2-α1-β2/3-α1-γ2	β3-α1-γ2-β2/3-α2	β3-α1-γ2-β2/3-α2	β2-α1-β1-α2-γ2	β2-α1-β1-β1-γ2	β2-α1-β2-α1-γ2
Model	β2-α1-β3-α1-γ2	β3-α1-γ2-β2-α2	β3-α1-γ2-β3-α2	β2-α1-β1-α2-γ2	β2-α1-β1-β1-γ2	β2-α1-β2-α1-γ2
EMDB ID	EMD-45983	EMD-45985	EMD-45980	EMD-45984	EMD-45986	EMD-47132
PDB ID	9CXA	9CXC	9CX7	9CXB	9CXD	9DRX
Initial model used (PDB code)	6X3T/6I53	6X3T/6I53	6X3T/6I53	6X3T/6I53	6X3T/6I53	6X3Z
Final particle images (no.)	74,535	29,584	29,584	30,789	28,909	124,678
Map resolution (Å) FSC threshold=0.143	3.04	3.30	3.30	3.33	3.36	2.95
Map sharpening *B* factor ($Å^2$)	89.4	80.6	80.6	79.7	76.9	83.5
Model composition						
Non-hydrogen atoms	16521	14, 577	14, 584	14, 479	15, 403	17, 398
Protein residues	1989	1754	1755	1749	1874	2121
Glycans	20	19	19	19	9	21
Ligands	4	4	4	2	2	3
Lipids	2	0	0	1	0	0
***B* factors ($Å^2$)**						
Protein	73.25	89.62	92.88	97.43	94.68	143.57
Ligands	94.65	111.21	116.73	96.22	111.31	133.19
R.m.s. deviations						
Bond lengths (Å)	0.006	0.005	0.007	0.006	0.004	0.008
Bond angles (°)	0.936	0.755	1.112	0.950	0.896	1.232
Validation						
MolProbity score	1.59	1.49	2.10	1.74	1.61	1. 7 1
Clashscore	5.50	4.10	8.10	6.38	5.18	5. 03
Poor rotamers (%)	1.0	0.06	2.23	1.0	0.42	1.43
Ramachandran plot						
Favored (%)	95.82	95.79	94.17	94.33	95.14	95.39
Allowed (%)	4.18	4.21	5.83	5.67	4.86	4.61
Disallowed (%)	0	0	0	0	0	0

Table summarizing cryo-EM data refinement and validation statistics for 5 of the native receptor maps and models, and for the recombinant receptor plus lamotrigine map and model, generated in this study.

nature portfolio

Corresponding author(s): Ryan Hibbs

Last updated by author(s): Nov 8, 2024

Reporting Summary

Nature Portfolio wishes to improve the reproducibility of the work that we publish. This form provides structure for consistency and transparency in reporting. For further information on Nature Portfolio policies, see our Editorial Policies and the Editorial Policy Checklist.

Statistics

For all statistical analyses, confirm that the following items are present in the figure legend, table legend, main text, or Methods section.

n/a	Confirmed	
☐	☒	The exact sample size (*n*) for each experimental group/condition, given as a discrete number and unit of measurement
☐	☒	A statement on whether measurements were taken from distinct samples or whether the same sample was measured repeatedly
☐	☒	The statistical test(s) used AND whether they are one- or two-sided *Only common tests should be described solely by name; describe more complex techniques in the Methods section.*
☒	☐	A description of all covariates tested
☒	☐	A description of any assumptions or corrections, such as tests of normality and adjustment for multiple comparisons
☐	☒	A full description of the statistical parameters including central tendency (e.g. means) or other basic estimates (e.g. regression coefficient) AND variation (e.g. standard deviation) or associated estimates of uncertainty (e.g. confidence intervals)
☐	☒	For null hypothesis testing, the test statistic (e.g. *F*, *t*, *r*) with confidence intervals, effect sizes, degrees of freedom and *P* value noted *Give P values as exact values whenever suitable.*
☒	☐	For Bayesian analysis, information on the choice of priors and Markov chain Monte Carlo settings
☒	☐	For hierarchical and complex designs, identification of the appropriate level for tests and full reporting of outcomes
☒	☐	Estimates of effect sizes (e.g. Cohen's *d*, Pearson's *r*), indicating how they were calculated

Our web collection on statistics for biologists contains articles on many of the points above.

Software and code

Policy information about availability of computer code

Data collection	pClamp11
Data analysis	GraphPad Prism 10.2, ClampFit 11, Coot 0.9.8.92, Phenix 1.20.1, cryoSPARC 4.4, UCSF CimeraX 1.7.1, Molprobity V4.5, Hole 2, Pymol 2.5.5

For manuscripts utilizing custom algorithms or software that are central to the research but not yet described in published literature, software must be made available to editors and reviewers. We strongly encourage code deposition in a community repository (e.g. GitHub). See the Nature Portfolio guidelines for submitting code & software for further information.

Data

Policy information about availability of data

All manuscripts must include a data availability statement. This statement should provide the following information, where applicable:

- Accession codes, unique identifiers, or web links for publicly available datasets
- A description of any restrictions on data availability
- For clinical datasets or third party data, please ensure that the statement adheres to our policy

All atomic models and cryo-EM maps have been deposited in the Protein Data Bank and Electron Microscopy Data Bank: β2-α1-β2-α1-γ2 (PDB 9CRS, EMD 45878), β2-α1-γ2-β2-α2 (PDB 9CRV, EMD 45884), β3-α1-β2-α2-γ2 (PDB 9CSB, EMD 45890), β2-α1-β2-α2-γ2 (PDB 9CT0, EMD 45894), β2-α1-β3-α2-γ2 (PDB 9CTJ, EMD 45908), β2-α1-β2-α3-γ2 (PDB 9CTP, EMD 45914), β2-α1-γ2-β1-α2 (PDB 9CTV, EMD 45920), β2-α1-β3-α1-γ2 (PDB 9CXA, EMD 45983), β3-α1-γ2-β2-α2 (PDB 9CXC,

EMD 45985), β3-α1-γ2-β3-α2 (PDB 9CX7, EMD 45980), β2-α1-β1-α2-γ2 (PDB 9CXB, EMD 45984), β2-α1-β1-β1-γ2 (PDB 9CXD, EMD 45986), LTG bound β2-α1-β2-α1-γ2 (PDB 9DRX, EMD 47132) . Raw electrophysiology and mass spectrometry results are included as Source data with the paper.

Research involving human participants, their data, or biological material

Policy information about studies with human participants or human data. See also policy information about sex, gender (identity/presentation), and sexual orientation and race, ethnicity and racism.

Reporting on sex and gender	This study included 32 females and 49 males. Sex was determined based on participant's medical chart. No sex- or gender-based analyses were performed in the study as they were not part of hypotheses being tested.
Reporting on race, ethnicity, or other socially relevant groupings	n/a
Population characteristics	Population characteristics are presented in detail in Extended Data tables 1 and 2.
Recruitment	Participants were adult patients undergoing resection as part of a standard clinical procedure for the treatment of pharmacologically resistant epilepsy at the University of Texas Southwestern Medical Center (UTSW). Potential participants were identified when they presented to the clinic for evaluation for seizure surgery. The standard course of seizure surgery evaluation at UTSW includes the presentation of each patient case to an interdisciplinary team of physicians which reviews the case details to determine whether the patient is a good candidate for surgical intervention. If these evaluations determined that surgical resection was the appropriate clinical course, the potential participants were approached about contributing to the study. Informed consent was obtained prior to surgery. Patients were recruited regardless of race, ethnicity, or sex.
Ethics oversight	The protocol was approved by the UTSW Institutional Review Board on Human subjects Research prior to tissue collection. All participants provided informed written consent.

Note that full information on the approval of the study protocol must also be provided in the manuscript.

Field-specific reporting

Please select the one below that is the best fit for your research. If you are not sure, read the appropriate sections before making your selection.

☒ Life sciences ☐ Behavioural & social sciences ☐ Ecological, evolutionary & environmental sciences

For a reference copy of the document with all sections, see nature.com/documents/nr-reporting-summary-flat.pdf

Life sciences study design

All studies must disclose on these points even when the disclosure is negative.

Sample size	Tissue sample size was determined empirically based on amount needed to obtain structural information. Amount of cryo-EM data was limited by time limitation on microscopes and by reaching sufficient resolution to model protein structures. For patch clamp electrophysiology, we selected healthy looking cells. We selected cells also based on GFP fluorescence from co-transfection with this plasmid. No statistical tests were used to predetermine the sample size but all measurements were performed using 3-10 biologically independent samples (cells). Sample sizes for electrophysiology were chosen to assess reproducibility.
Data exclusions	Tissues from patients with cortical dysplasia or other structural abnormalities, or tumors, were excluded from this study. cryoSPARC-based 2D and 3D classification of single particle datasets were used to remove junk particles.
Replication	All attempts at replication were successful. Cryo-EM datasets were collected over 24-72 hr and were consistent from the beginning to the end. Electrophysiology experiments were performed on at least three independent transfections across multiple days of experiments.
Randomization	Samples were nor randomized as it is not practically feasible to do so for cryo-EM or patch clamp electrophysiology studies. Covariant control was also not possible in in patch clamp experiments because of the need to transfect cells with predetermined cDNAs and optimize protein expression for individual constructs.
Blinding	Researchers were not blinded during biochemistry and structural analyses, however they were blinded as to patient tissue location and patient sex, gender and age until structural analysis was complete. It is neither technically nor practically feasible to blind researchers for cryo-EM or electrophysiological experiments. It is not economically viable to blind cryo-EM data collections as additional naive staff would have to be recruited. For electrophysiology, the same researchers were in charge of molecular biology, cell culture, and recording, which was necessary to achieve high quality results. These situations made blinding in the structural components impossible.

Reporting for specific materials, systems and methods

We require information from authors about some types of materials, experimental systems and methods used in many studies. Here, indicate whether each material, system or method listed is relevant to your study. If you are not sure if a list item applies to your research, read the appropriate section before selecting a response.

Materials & experimental systems

n/a	Involved in the study
☐	☒ Antibodies
☐	☒ Eukaryotic cell lines
☒	☐ Palaeontology and archaeology
☒	☐ Animals and other organisms
☒	☐ Clinical data
☒	☐ Dual use research of concern
☒	☐ Plants

Methods

n/a	Involved in the study
☒	☐ ChIP-seq
☒	☐ Flow cytometry
☒	☐ MRI-based neuroimaging

Antibodies

Antibodies used: 1F4 Fab against the alpha1 subunit of the GABAA receptor was characterized by our group previously as referenced in the Methods section. For example details on this monoclonal antibody, see PMIDs 38898000 and 29950725. For the current study, we produced this antibody fragment recombinantly.

Validation: Binding was validated by gel filtration and structural analysis; sequence was verified through DNA sequencing of the expression construct and by the experimental density map.

Eukaryotic cell lines

Policy information about cell lines and Sex and Gender in Research

Cell line source(s): ExpiCHO cells-from Thermo Fisher (A29127), HEK293 GnTI- from ATCC (CRL-3022)

Authentication: Thermo Fisher provided the ExpiCHO cell line and used STR profiling. ATCC provided the HEK cell line and used STR profiling.

Mycoplasma contamination: The ExpiCHO and HEK cell lines tested negative for mycoplasma by the provider (Thermo Fisher, ATCC) and were not retested in the lab.

Commonly misidentified lines (See ICLAC register): No commonly misidentified cell lines were used in this study.

Plants

Seed stocks: n/a

Novel plant genotypes: n/a

Authentication: n/a